Bioconjugate Chemistry

pubs.acs.org/bc
Article

High-Affinity NIR-Fluorescent Inhibitors for Tumor Imaging via Carbonic Anhydrase IX

Gediminas Žvinys, Agne Petrosiute, Audrius Zakšauskas, Asta Zubrienė, Alvilė Ščerbavičienė, Zane Kalnina, Edita Capkauskaitė, Vaida Juozapaitienė, Aurelija Mickevičiūtė, Kirill Shubin, Švitrigailė Grincevičienė, Steponas Raišys, Kaspars Tars, Jurgita Matulienė, and Daumantas Matulis*

Cite This: *Bioconjugate Chem.* 2024, 35, 790–803

Read Online

ACCESS | Metrics & More | Article Recommendations | Supporting Information

ABSTRACT: Tumor imaging and delivery of therapeutic agents may be achieved by designing high-affinity and high-selectivity compounds recognizing a tumor cell-expressing biomarker, such as carbonic anhydrase IX (CA IX). The CAIX, overexpressed in many hypoxic solid tumors, helps adjust to the energy requirements of the hypoxic environment, reduces intracellular acidification, and participates in the metastatic invasion of adjacent tissues. Here, we designed a series of sulfonamide compounds bearing CAIX-recognizing, high-affinity, and high-selectivity groups conjugated via a PEG linker to near-infrared (NIR) fluorescent probes used in the clinic for optically guided cancer surgery. We determined compound affinities for CAIX and other 11 catalytically active CA isozymes by the thermal shift assay and showed that the affinity K_d value of CAIX was in the subnanomolar range, hundred to thousand-fold higher than those of other CA isozymes. Similar affinities were also observed for CAIX expressed on the cancer cell surface in live HeLa cell cultures, as determined by the competition assay. The NIR-fluorescent compounds showed excellent properties in visualizing CAIX-positive tumors but not CAIX-negative knockout tumors in a nude mice xenograft model. These compounds would therefore be helpful in optically guided cancer surgery and could potentially be developed for anticancer treatment by radiotherapy.

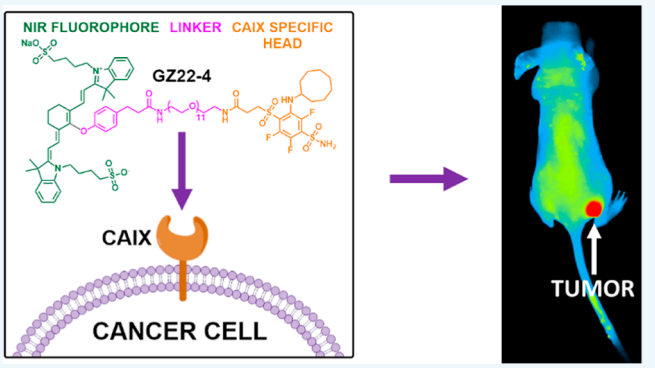

1. INTRODUCTION

The development of theranostic fluorescence imaging agents and radiopharmaceuticals is an important trend in cancer diagnosis and treatment,[1] and selecting a specific cancer-related protein target is essential for success. Tumor hypoxia is a predictor of worse outcomes and treatment resistance in a variety of solid tumors. Characterization and detection of hypoxic regions within solid tumor masses are important tasks. Therefore, a molecular imaging application, targeting proteins that serve as markers for tumor hypoxia is needed. Such imaging could help decide which patients will benefit from hypoxia-targeting therapy and help detect and follow the treatment response of the disseminated metastatic disease.[2]

An increased expression of carbonic anhydrase IX (CAIX) has been noted in a variety of cancers,[3] and the development of CAIX recognition-based theranostic radiopharmaceuticals has become an attractive research venue.[1] Numerous CAIX-targeted radionuclide therapy agents are currently undergoing various phases of clinical trials.[4] This interest stems from their unique characteristics, in which chemically identical entities can be used for diagnosis and cancer treatment by incorporating various radionuclides. The most suitable design approach, proven in the field of CAIX-targeting theranostic molecules, involves the formation of a conjugate between an effective CAIX inhibitor and a metal chelator, tethered with a suitable linker.[5] The ideal radiotracer must have high sensitivity and high specificity for CAIX-positive metastases. Small molecules are promising for therapeutic radiopharmaceuticals (^{177}Lu, ^{161}Tb, ^{225}Ac, ^{212}Pb, and others) since myelotoxicity is observed in most patients treated with a radioimmunoconjugate.[6] While most studies with small-molecule conjugates are preclinical, several tracers have been tested in clinical trials[7,8] with notable off-target uptake of these compounds related to nonspecific CA binding of acetazolamide. Therefore, more specific and more sensitive CAIX-recognizing radiotracer molecules are needed.

The first step in developing such theranostic agents should involve the design and synthesis of a highly specific CAIX-recognizing compound. Our laboratory has designed a number

Received: March 29, 2024
Revised: April 25, 2024
Accepted: April 25, 2024
Published: May 15, 2024

Scheme 1. Chemical Structures of Compounds Bearing a CAIX-Recognizing Headgroup (on the Left of the Structure), a PEG-Containing Linker (Pink), and an NIR-Fluorescent Group (Green, on the Right of the Compound)

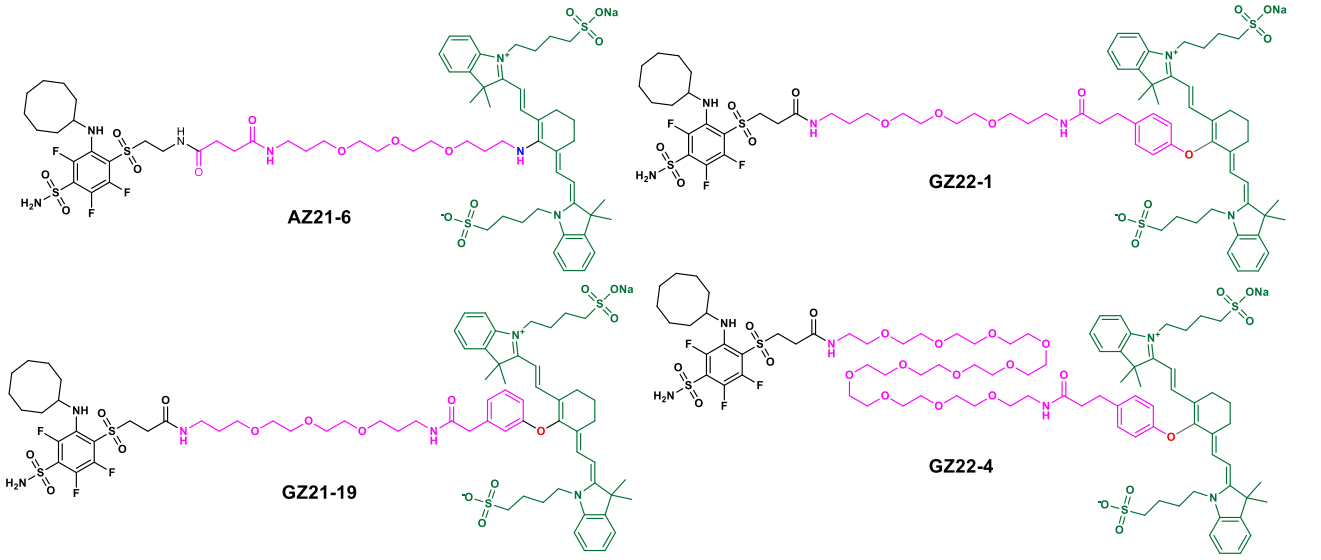

of such candidate compounds.[9−11] We have selected the most promising compounds and tagged them to the NIR-fluorescent probes as the first step in assessing the specificity and biodistribution of these candidate probes for further development. Next, we assessed the targeting abilities of the new CAIX-specific NIR molecules in vitro and in vivo. We showed here that CAIX-recognizing compounds conjugated with NIR-fluorescent probes resulted in suitable probes for CAIX-positive tumor visualization in mice xenograft models.

2. RESULTS

2.1. Design of High-Affinity Selective NIR-Fluorescent Inhibitors of CAIX. In search of ligands with high selectivity and affinity toward cancer-associated CAIX, our laboratory previously designed, synthesized, and tested over 1000 sulfonamide compounds. One of them, VD11-4-2, demonstrated a very strong binding affinity to CAIX (dissociation constant K_d = 30 pM) and remarkable selectivity over other CA isozymes.[9] To make our inhibitor suitable for cancer imaging, we synthesized a compound **AZ21-6** that bears an NIR-783 fluorophore attached to the inhibitor via a 3-mer polyethylene glycol linker chain (marked in pink) via an amine group (marked in blue) (Scheme 1). Three additional compounds **GZ21-19**, **GZ22-1**, and **GZ22-4** were synthesized with oxygen instead of nitrogen connecting the NIR-783 fluorophore with the linker. We expected oxygen to have an impact on compounds' NIR-fluorescence properties[12,13] and not undergo a pH-related hypsochromic shift as reported with nitrogen compounds.[14] Spectrophotometric data confirmed the desired bathochromic shift with all three compounds (Figure S1), and a stronger fluorescence response was also observed (Table S1). Compound **GZ22-4** was synthesized with a longer PEG linker of 11-mer than other compounds. A longer linker may be needed for a stronger fluorescence signal because of CAIX's dimeric nature and potential shielding of the fluorophore connected with a short linker to the inhibitor while bound to an active site.[15] A longer linker could provide the fluorophore with more flexibility and the ability to distance itself further from the protein. As expected, the compound **GZ22-4** was more brightly fluorescent than the other three compounds (Figure S4).

The synthesis of NIR-fluorescent compounds was carried out as shown in Scheme 2. The inhibitor **GZ18-23** and compounds leading to it were prepared by previously described procedures.[16] The 3-mer and 11-mer PEG linkers were introduced via amide coupling. TFA and DCM were used for amine deprotection, yielding compounds **GZ21-10** and **GZ22-3**. The commercial NIR783 dye was coupled with phenolic alkyl acids. Final GZ compounds were acquired by amide coupling between phenolic NIR783 conjugates and PEGylated inhibitors. **AZ21-1B** was coupled with a 3-mer PEG linker via amide bond formation. Similarly, TFA and DCM were used for amine-group deprotection and subsequently coupled with NIR783, yielding the final **AZ21-6** compound.

2.2. Binding of NIR Inhibitors to CAIX and Other Recombinant Human CA Isozymes. The binding affinities of the four NIR-fluorescent compounds to 12 catalytically active recombinant CA isozymes were determined by the fluorescence-based thermal shift assay (FTSA), and the dissociation constants (K_d's) at physiological pH (pH 7.0) and 37 °C are listed in Table 1. The curves of **GZ22-4** binding to CAIX are shown in Figure 1.

The thermal shift assay results show that all four NIR-fluorescent compounds bound with subnanomolar affinity to CAIX. A bulky PEG tail containing a NIR-fluorescent moiety only slightly diminished the affinity, as compared to a compound that does not possess the bulky group. In addition, all four compounds possessed high selectivity for CAIX over all the 11 remaining catalytically active human CA isozymes. Selectivity for binding CAIX over CAI, CAIII, CAIV, and CAVA exceeded 10,000-fold, while the selectivity over CAII, CAVB, CAVI, CAVII, CAXII, and CAXIV exceeded 100-fold and that over CAXIII exceeded 20-fold. Therefore, all four NIR-fluorescent compounds were high-affinity and strong-selectivity ligands suitable for further application for visualization of CAIX in cell cultures and live animals.

2.3. NIR-Fluorescent Inhibitor Binding to Live HeLa Cells Expressing CAIX. To measure NIR-fluorescent compound binding to CAIX expressed in cancer cells, the

https://doi.org/10.1021/acs.bioconjchem.4c00144
Bioconjugate Chem. 2024, 35, 790−803

Scheme 2. Scheme of the Synthesis of NIR-Fluorescent Compound

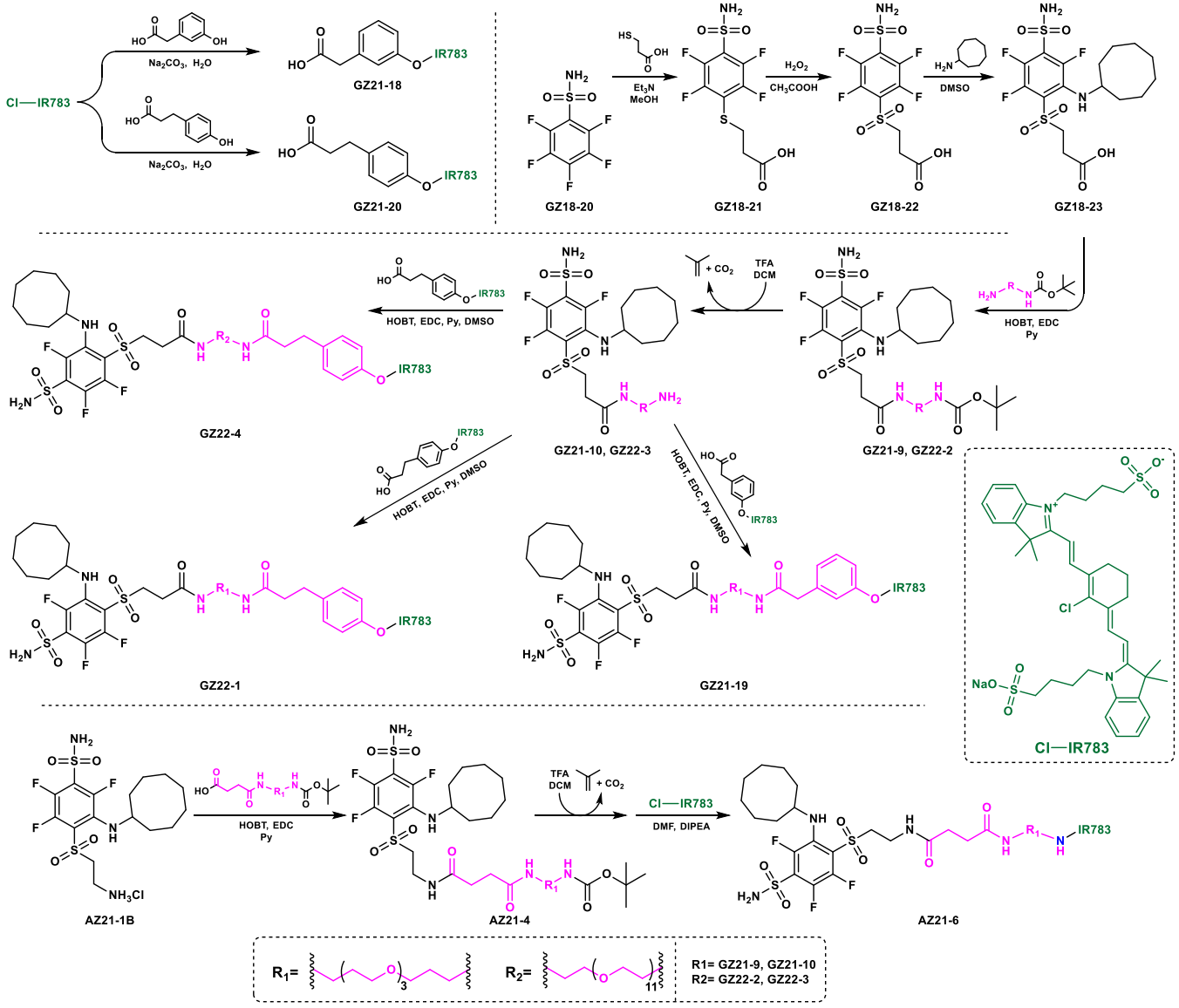

Table 1. Dissociation Constants K_d's (in nM Units) for the Interaction of Compounds with Human Recombinant CA Isozymes as Determined by FTSA at 37 °C and pH 7.0[a]

compound	K_d, nM											
	CAI	CAII	CAIII	CAIV	CAVA	CAVB	CAVI	CAVII	**CAIX**	CAXII	CAXIII	CAXIV
AZ21-6	20,000	2000	30,000	8000	10,000	50	1000	60	**0.3**	50	10	100
GZ21-19	10,000	400	20,000	2000	2000	ND	700	ND	**0.2**	60	ND	100
GZ22-1	ND	20	30,000	7000	1000	ND	700	30	**0.3**	200	8	100
GZ22-4	ND	200	5000	8000	2000	ND	500	40	**0.2**	80	5	90
GZ18-23	5000	200	≥200,000	100	10,000	200	100	40	**0.03**	1.4	10	3

[a]ND—not determined. The K_d values for **GZ18-23** were taken from ref 16.

GZ22-4 compound was applied in different concentrations to live HeLa cells grown under hypoxia and normoxia, as described in the Materials and Methods section, and was previously performed for the fluorescein-conjugated CAIX inhibitor **GZ19-32**.[16] In contrast to **GZ19-32**, **GZ22-4** compound showed no difference in the fluorescence signal in hypoxia vs normoxia, most likely due to the lower fluorescence quantum yield of NIR dye as compared to fluorescein. The difference was hidden in the low signal-to-noise ratio.

To increase the amount of CAIX expression, the HeLa cells were transfected with the CAIX-encoding plasmid pCMV-CAIX. There was a dramatic increase in CAIX expression observed both in the dosing curve and fluorescence microscopy results. Figure 2A shows the dosing curves of **GZ22-4** obtained with the transfected and nontransfected HeLa cell cultures. In the case of transfection, we can see both the specific CAIX-dependent signal and relatively weak nonspecific binding of the dye to unknown targets at

https://doi.org/10.1021/acs.bioconjchem.4c00144
Bioconjugate Chem. 2024, 35, 790−803

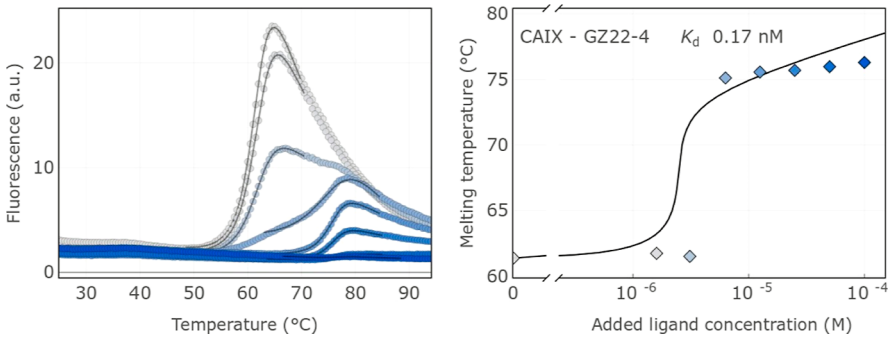

Figure 1. Determination of NIR-fluorescent compound binding affinities by the thermal shift assay [panels (A) and (B)]. (A) Fluorescence melting curves of CAIX at various concentrations of the added compound **GZ22-4**. (B) Dosing curve showing the T_m dependence on the compound concentration. The fit is performed automatically yielding the K_d. Note that the data points near the inflection are not important for the curve fit to obtain a reliable K_d.[17]

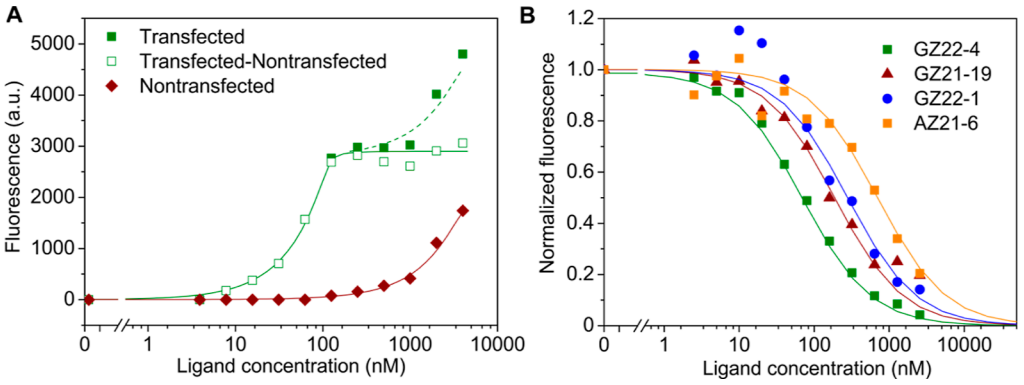

Figure 2. (A) Dosing curves with the NIR-fluorescent **GZ22-4** compound of HeLa cell culture grown for 2 days under normoxia, nontransfected (brown filled diamonds) or transfected with the CAIX-encoding plasmid (green filled squares). Nonspecific binding of the dye is visible at high concentrations exceeding approximately 1 μM for both transfected and nontransfected cell cultures. Specific CAIX binding is seen only for transfected cells. Subtraction of nontransfected from transfected fluorescence values yielded open data points, fit to the regular dosing model (solid green line). The fit shows that there is 120 nM CAIX concentration in the cell culture. (B) Determination of affinities of compounds **GZ22-4** (green squares), **GZ21-19** (red triangles), **GZ22-1** (blue circles), and **AZ21-6** (orange squares) for cell-expressed CAIX via a competition assay with the fluorescein-labeled **GZ19-32** compound. The cells were grown under hypoxia and not transfected because fluorescence properties of **GZ19-32** were sufficient to determine CAIX expression in hypoxic cells.

concentrations above approximately 1 μM (shown as a dashed curve, increasing at the same concentrations as the nontransfected cell dosing curve).

Fluorescence values corresponding to the transfection effect were obtained by subtraction of nontransfected values from transfected fluorescence values, showing the resultant data points as open squares. These data were fit to a regular dosing curve yielding the CAIX concentration 120 nM and K_d equal to 1 nM. These data match well with the K_d obtained by FTSA for purified CAIX, equal to 0.2 nM. However, the determination of the K_d via dosing curves at such high protein concentrations is not accurate and can only serve as an estimate of affinity.

2.4. Affinities of NIR-Fluorescent Compounds for Cells Expressing CAIX by the Competition Assay. Hypoxia-grown HeLa cell culture expressed approximately 2 nM CAIX, which was quantified by fluorescein-labeled **GZ19-32** added at a constant concentration of 10 nM throughout the assay. The four NIR-fluorescent compounds were dosed and competed with the **GZ19-32** compound in a dose-dependent manner. At high concentrations, all four compounds fully outcompeted the fluorescein-bearing compound yielding nice competition curves (Figure 2B). Each curve was fit using the total protein CAIX (P_t) value of 2 nM, and the K_d of **GZ19-32** was 200 pM. The dissociation constants for each NIR-fluorescent compound were 4 nM for **GZ21-19**, 6 nM for **GZ22-1**, 1.5 nM for **GZ22-4**, and 15 nM for **AZ21-6**. Thus, compound affinities were similar but not identical, despite having identical headgroups. The differences in the tail length and chemical structure must have caused the small differences in affinities, where **GZ22-4** showed the highest affinity and **AZ21-6** the lowest affinity of the four. The affinity of fluorescein-bearing **GZ19-32** was the highest of all, around 200 pM.

Note that there was no need for transfection for the competition assay because the levels of hypoxia-induced CAIX were sufficient to be quantified by highly fluorescent **GZ19-32**. However, the NIR compounds could not be used to quantify CAIX expressed in cells grown under hypoxia in the plate reader because fluorescence detection was too low in the NIR region. The NIR-fluorescent compounds did not interfere with readings in the green fluorescence range since they fluoresce in the NIR region around 850 nm, while **AZ21-6** has fluorescence maximum around 780 nm.

2.5. Microscopy of the NIR-Fluorescent Compound Staining of CAIX-Expressing Human Cancer Cells. Live HeLa cell culture was used for visualization of the NIR-fluorescent compound binding to CAIX expressed on cell

https://doi.org/10.1021/acs.bioconjchem.4c00144
Bioconjugate Chem. 2024, 35, 790−803

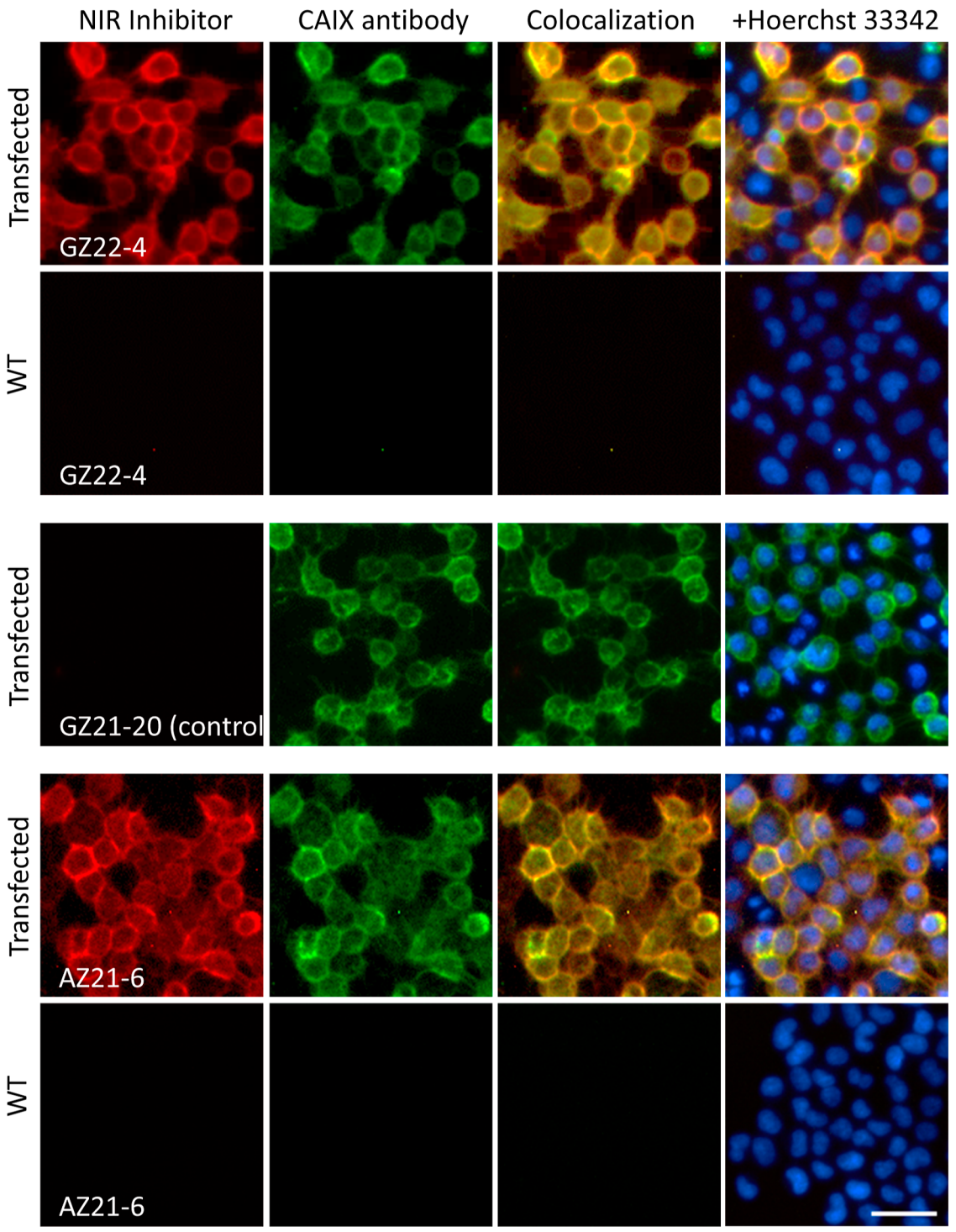

Figure 3. Staining of live HeLa cells grown under normoxia (wild type and transfected with CAIX-encoding DNA) and incubated with 250 nM NIR inhibitors (**GZ22-4**, **AZ21-6**) and control compound **GZ21-20** that does not contain the CAIX-recognizing headgroup. Beginning from the left, the columns show the binding of NIR inhibitors (red), CAIX antibody (green), colocalization of NIR compounds and CAIX antibody (first two columns), and colocalization overlaid with cell nuclei (Hoerchst 33342, blue). Due to approximately 80% transfection efficiency, some cells remained untransfected and showed no antibody or compound binding. Scale bar length is 40 μm.

membranes (Figures 3 and S2). All four CAIX-selective compounds (**GZ22-4**, **AZ21-6**, **GZ21-19**, and **GZ22-1**) stained the membranes of pCMV-CAIX-transfected cells, while wild-type cells, grown both under normoxia and hypoxia, gave no visual signal (1st column, Figures 3 and S2). Hypoxic conditions were insufficient for CAIX-specific fluorescence detection (Figure S3). Transfected cells expressed 10-fold more CAIX protein than cells grown under hypoxia, as determined by dosing the fluorescein-containing compound **GZ19-32**. The control compound **GZ21-20** that does not have CAIX-specific inhibitor headgroup shows no visual response on transfected cells (Figure 3). The second column shows cell staining with the CAIX antibody, which colocalized with the staining of NIR-fluorescent compounds (3rd column). The

https://doi.org/10.1021/acs.bioconjchem.4c00144
Bioconjugate Chem. 2024, 35, 790−803

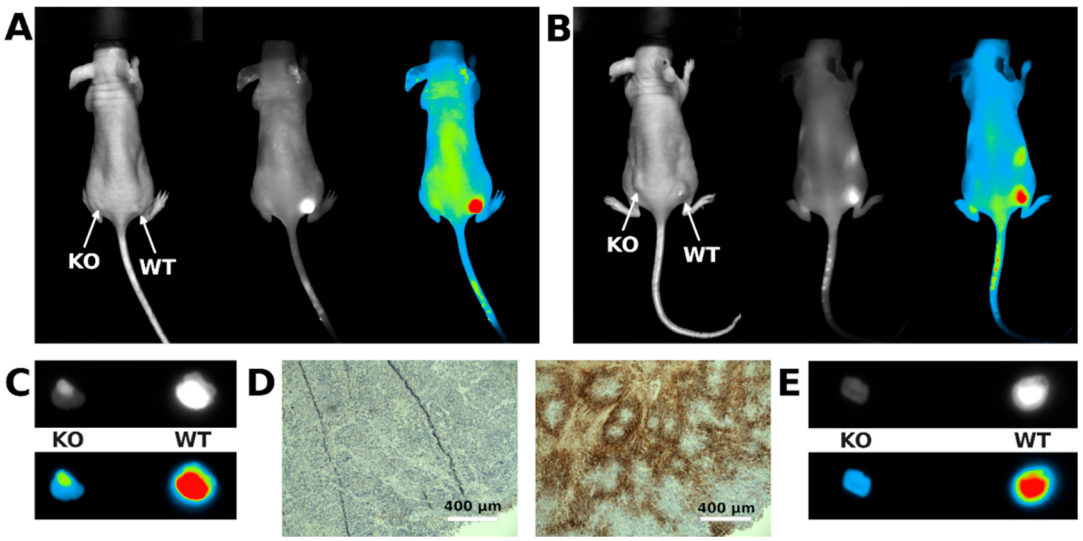

Figure 4. GZ22-4 and **AZ21-6** distribution patterns in nude mice with Hela xenograft. (A) **GZ22-4** compound uptake in nude mice bearing HeLa CAIX^{WT} tumors injected into the right flank compared to HeLaCAIX^{KO} tumors, injected into the left flank. (B) **AZ21-6** compound uptake in nude mice bearing HeLa CAIX^{WT} tumors injected into the right flank compared to HeLaCAIX^{KO} tumors, injected into the left flank. (C) **GZ22-4** compound uptake differences in HeLa CAIX^{WT} compared to HeLaCAIX^{KO} tumors ex vivo. Images were obtained 3 days after dye injection. (D) Immunohistochemistry of HeLaCAIX^{WT} versus HeLaCAIX^{KO} line xenograft tumor samples reveal the absence of CAIX staining in HeLa CAIX^{KO} tumors compared to HeLaCAIX^{WT}. Scale bars, 400 μm. (E) **AZ21-6** compound uptake differences in HeLa CAIX^{WT} compared to HeLaCAIX^{KO} tumors ex vivo. Images were obtained 7 days after dye injection.

fourth column shows the overlay of colocalization with the staining of cell nuclei. The **GZ22-4** showed the best fluorescence signal as compared to the other three compounds if images were taken at identical exposure conditions (Figure S4). We should point out that microphotographs in Figures 3 and S2 were taken at different exposure times to ensure good visualization quality. Nevertheless, all four compounds were suitable for direct visualization of CAIX expressed on transfected cell membranes.

2.6. CAIX-Expressing Tumor Imaging in HeLa Xenograft-Based Mice. Recognition of CAIX-expressing tumors by a specific NIR probe in vivo requires a suitable xenograft platform. Previously, our laboratory has developed a CAIX-knockout HeLa cell line (HeLa CAIX^{KO}), confirmed by sequencing and several antibody-based detection methods[16].

The HeLaCAIX^{WT} and HeLaCAIX^{KO} cells were injected subcutaneously (S.Q.) into opposite flanks of nude mice, 3×10^6 cells per injection. Once tumors reached the palpable size, we performed imaging using the UVITEC AllianceQ9 Imager system. The images were obtained every 24 h after intravenous (I.V.) compound injection into a tail vein. To analyze fluorescent compound uptake, two best candidate compounds were chosen, **AZ21-6** and **GZ22-4**. Compound **GZ22-4** was selected because of the photostability and good quantum yield (Table S1), and the fluorescence maximum of **AZ21-6** closely resembled the center of the NIR filter of the imaging system. Both compounds had the best solubility properties and good in vitro binding to cells. We saw a preferential uptake of the compound in HeLaCAIX^{WT} tumors compared to HeLa-CAIX^{KO} tumors when using both compounds (Figure 4A,B). The **GZ22-4** NIR compound seemed to be slightly more specific toward CAIX, consistent with the highest affinity for CAIX (Figure 2) and had a faster clearance from nontumor locations based on daily images.

3. DISCUSSION

The NIR-fluorescent compounds described in this study bound to CAIX with the highest affinity for CAIX among all small-molecule compounds described in the literature. Taking into account their high selectivity for CAIX over remaining CA isozymes makes them highly preferable for CAIX tumor visualization. Chemically, the compounds are rather simple to synthesize, and they have good physicochemical properties such as aqueous solubility.

Affinity together with selectivity is the main reason why these compounds in the in vivo study showed so significantly different uptake of CAIX-NIR compounds in HeLaCAIX^{WT} tumors as compared to HeLaCAIX^{KO} tumors. It is important to emphasize that both tumors were in the same mouse, making the effect independent of individual mouse variation. The NIR-fluorescent compounds were specific toward CAIX and at the shown times labeled specifically the WT tumor bearing CAIX. Furthermore, based on the mice daily images, they had a relatively fast clearance from nontumor organs. Still, there was somewhat prolonged accumulation of both tested compounds in the liver and kidney. Despite quite high selectivity, the headgroup recognizing CAIX that bears the cyclo-octyl ring was not completely selective for CAIX. Several other CA isozymes bound the compounds with nanomolar affinity, among which are CAII, CAVB, CAVII, CAXII, CAXIII, and CAXIV. Some of those interactions, especially with CAXII, could be beneficial, but others may lead to nonspecific binding to other CA isozymes and staining nontumor tissues if applied at concentrations exceeding the CAIX amount in the tumor. Thus, a further increase in selectivity could be beneficial for such compound application in theranostics of CAIX-positive cancers.

Since the discovery of CAIX as a hypoxic tumor biomarker,[18−20] numerous studies have used antibodies, small-molecule compounds, and nanoparticles conjugated to fluorescent or radioactive elements designed both for tumor

https://doi.org/10.1021/acs.bioconjchem.4c00144
Bioconjugate Chem. 2024, 35, 790−803

imaging and cancer treatment.[1−3,5,14,21−54] Several small-molecule probes have reached clinical trials. For instance, ^{18}F-VM4-037, a small-molecule radiotracer developed on the sulfonamide pharmacophore, a derivative of the CA ligand ethoxzolamide, failed to localize the ccRCC tumor as it had a high background in the kidney and liver.[29] This was partially due to ethoxzolamide-limited selectivity for CAIX over other CA isozymes. The study with a ^{99m}Tc-labeled acetazolamide derivative, ^{99m}Tc-PHC-102, showed encouraging results in a pilot study using a SPECT/CT scanner for identifying substantial tumor and metastasis uptake. However, some gallbladder and stomach uptake was noted.[7] A pilot study of ^{68}Ga-NY104, based on an acetazolamide core and connected to a hydrophilic spacer and a chelator NOTA in 3 patients with ccRCC showed excellent tumor uptake and a high ratio of tumor-to-background. Non-negligible uptake in the kidney, stomach, intestine, lung, and liver was also noted.[8] Most of the conjugated compounds were based on an acetazolamide or a benzenesulfonamide headgroup that possesses limited selectivity for CAIX. The main issue appeared to be insufficient affinity and the lack of selectivity in binding CAIX over other CA isozymes and potentially other proteins.

Contrary to our previously designed fluorescein-labeled compounds that nicely stained hypoxia-grown cell cultures and could be used to quantify the expression of the CAIX protein,[16] the same cells stained with the NIR fluorescent compounds did not show any detectable signal. This was due to limited capabilities of detection in the infrared wave region. We estimated that the fluorescence yield was 10-fold lower for NIR compounds compared to fluorescein-bearing **GZ19-32**. In addition, the Cy7 filter of the fluorescence microscope used for the study was not fully suited for the detection in the 850 nm wavelength region. However, the NIR-compound-stained tumors in mice were nicely visible due to a multilayer cell structure of the mice tumors and better-suited NIR detection filters of the mice imaging system.

The NIR-fluorescent compounds exhibited extremely high affinity, where the K_d was 0.2 to 0.3 nM as determined by the fluorescence thermal shift assay. In addition, compound affinities were determined by our previously developed competition assay performed with live cells.[16] The K_d values obtained by the competition assay showed somewhat lower affinities for cell-expressed CAIX than for purified CAIX. The difference was approximately 10-fold, which was likely caused by the presence of various factors and proteins in the growth medium and cells.

Such high affinity was possibly necessary for optimal imaging, but it delayed the clearance of the compound from nontumor areas, and thus it took several days for optimal visualization of the WT tumor. The balance between affinity and selectivity is crucial for successful imaging of the tumor. Sufficiently good imaging could also be obtained with probes exhibiting lower affinities for CAIX, as shown in numerous studies, thus explaining visualization results after applying nonselective benzenesulfonamide- or acetazolamide-based conjugated compounds for CAIX imaging. However, this could be shown only because CAIX is expressed on the cell surface, while other CA isozymes are inside cells, thus minimizing nonspecific interactions. In our opinion, compounds possessing higher affinity for CAIX and sufficient selectivity over remaining CA isozymes, such as **GZ22-4**, are advantageous to visualize CAIX-positive tumors and could be further developed by attaching PET probes, other radioactive elements, for both visualization and cancer treatment.

4. MATERIALS AND METHODS

4.1. Chemical Synthesis. All starting materials and reagents were commercial products and were used without further purification. Melting points of the compounds were determined in open capillaries on a Thermo Scientific 9100 Series and were uncorrected. Column chromatography was performed using silica gel 60 (0.040−0.063 mm, Merck). ^{1}H and ^{13}C NMR spectra were recorded on a Bruker Ascend 400 spectrometer (400 and 100 MHz, respectively) with TMS as an internal standard, and proton and carbon chemical shifts are expressed in parts per million (ppm) in the indicated solvent. ^{19}F NMR spectra were recorded on a Bruker Ascend 400 spectrometer (376 MHz) with $CFCl_3$ as an internal standard, and fluorine chemical shifts are expressed in parts per million (ppm) in the indicated solvent. Multiplicity was defined as s (singlet), d (doublet), t (triplet), q (quartet), dd (double doublet), ddd (double double doublet), m (multiplet), and br s (broad singlet). TLC was performed with silica gel 60 F254 aluminum plates (Merck) and visualized with UV light. High-resolution mass spectroscopy (HRMS) spectra were recorded by an Agilent TOF 6230 equipped with an Agilent Infinity 1260 HPLC system, in positive or negative electrospray ionization (ESI) mode. In the positive mode, isocratic elution of 95% acetonitrile w/5% of 1% formic acid solution in water (18.2 MΩ·cm@25 °C) was used, and in the negative mode 80% acetonitrile w/20% water at a flow rate of 0.300−0.500 mL/min was used. Absorption was measured using a PerkinElmer Lambda 950 spectrophotometer and a 1 mm fused silica cuvette. Emission was measured using a Hamamatsu PMA-12 multichannel spectrometer and a 1 mm fused silica cuvette at 45° excitation angle. Excitation source was an NKT Photonics FIANIUM-15 laser coupled to a SuperK SELECT multichannel filter working at 78 MHz repetition rate. The photoluminescence quantum yield was estimated by utilizing an integrating sphere (SphereOptics) coupled to the same PMA-12 CCD spectrometer via an optical fiber, where a 150 W xenon lamp (LOT-Oriel) coupled to a monochromator (Sciencetech Inc.) was used as an excitation source.

The synthesis of compounds **GZ18-20**, **GZ18-21**, **GZ18-22**, and **AZ21-1B** has been previously described in the literature.[16]

4.2. 3-((2-(Cyclooctylamino)-3,5,6-trifluoro-4-sulfamoylphenyl)sulfonyl)propanoic Acid (GZ18-23).[55] Purified with column chromatography (EtOAc/$CHCl_3$/AcOH, 49.5:49.5:1 v/v/v). Yield: 3.3 g, 54%; mp 143−144 °C; TLC (EtOAc/$CHCl_3$/AcOH, 49.5:49.5:1 v/v/v): R_f = 0.58.

4.3. General Procedure for the Syntheses of GZ21-9 and GZ22-2. A mixture of **GZ18-23** (200.0 mg, 0.42 mmol, 1 equiv for **GZ21-9**; 97.0 mg, 0.21 mmol, 1 equiv for **GZ22-2**), EDC (196.0 mg, 1.27 mmol, 3 equiv for **GZ21-9**; 90.0 mg, 0.58 mmol, 2.8 equiv for **GZ22-2**), HOBT (114.0 mg, 0.85 mmol, 2 equiv for **GZ21-9**; 58.6 mg, 0.43 mmol, 2.1 equiv for **GZ22-2**), *tert*-butyl(3-(2-(2-(3-aminopropoxy)ethoxy)-ethoxy)propyl)carbamate (203.0 mg, 0.63 mmol, 1.5 equiv) for **GZ21-9** or *tert*-butyl(35-amino-3,6,9,12,15,18,21,24,27,30,33-undecaoxapentatriacontyl)-carbamate (200.0 mg, 0.31 mmol, 1.5 equiv) for **GZ22-2**, and 5 mL of dry pyridine was stirred at room temperature under an argon atmosphere for 24 h. The reaction progress was monitored using TLC. Solvent was evaporated under reduced

https://doi.org/10.1021/acs.bioconjchem.4c00144
Bioconjugate Chem. 2024, 35, 790−803

pressure, the crude product was poured into saturated sodium chloride solution (10 mL), acidified until neutral pH, and extracted with ethyl acetate. The organic layer was washed with sat. sodium chloride solution and dried over sodium sulfate. The solvent was evaporated under reduced pressure, and the residue was purified with column chromatography.

4.4. *tert*-Butyl (17-((2-(Cyclooctylamino)-3,5,6-trifluoro-4-sulfamoylphenyl)sulfonyl)-15-oxo-4,7,10-trioxa-14-azaheptadecyl)carbamate (GZ21-9). TLC (EtOAc/AcOH, 99:1 v/v): R_f = 0.5. Purified with column chromatography ($CHCl_3$/EtOAc, 1:1 v/v, then 100% EtOAc). Yield: 0.12 g, 37%; mp 70−71 °C;

^{1}H NMR (400 MHz, DMSO-d_6): δ 1.37 (9H, s, *tert*-Bu), 1.42−1.70 (16H, m, cyclooctane (12H) and PEG NHCH$_2$C*H*$_2$ (4H)), 1.80−1.89 (2H, m, cyclooctane), 2.57 (2H, t, J = 7.1 Hz, C*H*$_2$CONH), 2.95 (2H, q, J = 6.7 Hz, PEG C*H*$_2$NHCOO), 3.01 (2H, q, J = 6.7 Hz, PEG CH$_2$CONHC*H*$_2$), 3.33−3.41 (4H, m (inside H_2O), NHCH$_2$CH$_2$C*H*$_2$), 3.48 (8H, m, OC*H*$_2$C*H*$_2$O), 3.74 (2H, t, J = 7.1 Hz, SO$_2$C*H*$_2$), 3.75−3.81 (1H, m, C*H* cyclooctane), 6.60 (1H, d, J = 8.3 Hz, N*H* cyclooctylamine), 6.73 (1H, t, J = 5.4, N*H*COO), 8.03 (1H, t, J = 5.5, CH$_2$CON*H*), 8.35 (2H, s, N*H*$_2$SO$_2$).

^{13}C NMR (100 MHz, DMSO-d_6): δ 23.27 (cyclooctane), 25.46 (cyclooctane), 27.21 (cyclooctane), 28.27 (*C*H$_2$CON), 28.71 (*tert*-Bu), 29.54 (*C*H$_2$CH$_2$NHCOO), 30.17 (CONHCH$_2$*C*H$_2$), 32.67 (cyclooctane), 36.49 (*C*H$_2$NHCOO), 37.68 (CONH*C*H$_2$), 53.11 (SO$_2$*C*H$_2$), 55.88 (*C*H cyclooctane, d, J(^{19}F−^{13}C) = 11.0 Hz), 68.35 (CH$_2$*C*H$_2$CH$_2$NHCOO), 68.55 (CONHCH$_2$*C*H$_2$CH$_2$), 69.98 (O*C*H$_2$CH$_2$O), 70.21 (OCH$_2$*C*H$_2$O), 77.88 (*C*(CH$_3$)$_3$), 114.72−114.98 (m, *C1*), 127.80−128.19 (m, *C4*), 135.27 (d, *C2*, J(^{19}F−^{13}C) = 14.3 Hz), 137.21 (dm, *C5*, J(^{19}F−^{13}C) = 242.3 Hz), 144.45 (d, *C3*, J(^{19}F−^{13}C) = 250.6 Hz), 146.22 (C6, dm, J(^{19}F−^{13}C) = 251.6 Hz), 156.04 (*C*OO), 168.16 (*C*ON);

^{19}F NMR (376 MHz, DMSO-d_6): δ −125.03 (C3−*F*, s), −133.90 (C5−*F*, dd, ^1J = 27.0 Hz, ^2J = 12.4 Hz), −150.62 (C6−*F*, dd, ^1J = 26.8 Hz, ^2J = 6.6 Hz).

HRMS (m/z): [M]$^+$ calcd for $C_{32}H_{54}F_3N_4O_{10}S_2^+$, 775.3228; found, 775.3251.

4.5. *tert*-Butyl (39-((2-(Cyclooctylamino)-3,5,6-trifluoro-4-sulfamoylphenyl)sulfonyl)-37-oxo-3,6,9,12,15,18,21,24,27,30,33-undecaoxa-36-azanonatriacontyl)carbamate (GZ22-2). TLC (acetone/EtOAc, 1:1 v/v): R_f = 0.15. Purified with column chromatography (acetone/EtOAc, 1:1 v/v → acetone → acetone/MeOH, 10:1 v/v). Yield: 0.14 g, 69%; mp 74−75 °C;

^{1}H NMR (400 MHz, DMSO-d_6): δ 1.37 (9H, s, *tert*-Bu), 1.42−1.69 (12H, m, cyclooctane), 1.79−1.89 (2H, m, cyclooctane), 2.60 (2H, t, J = 7.2 Hz, C*H*$_2$CONH), 3.06 (2H, q, J = 6.0 Hz, PEG C*H*$_2$NHCOO), 3.14 (2H, q, J = 5.8 Hz, PEG CH$_2$CONHC*H*$_2$), 3.47−3.52 (44H, m, PEG), 3.73 (2H, t, J = 7.2 Hz, SO$_2$C*H*$_2$), 3.75−3.82 (1H, m, C*H* cyclooctane), 6.60 (1H, d, J = 8.4 Hz, N*H* cyclooctylamine), 6.75 (1H, t, J = 5.8, N*H*COO), 8.15 (1H, t, J = 5.6, CH$_2$CON*H*), 8.35 (2H, s, N*H*$_2$SO$_2$);

^{13}C NMR (100 MHz, DMSO-d_6): δ 23.28 (cyclooctane), 25.46 (cyclooctane), 27.21 (cyclooctane), 28.22 (*C*H$_2$CON), 28.69 (*tert*-Bu), 32.69 (cyclooctane), 53.13 (SO$_2$*C*H$_2$), 55.88 (*C*H cyclooctane, d, J(^{19}F−^{13}C) = 11.1 Hz), 69.41 (PEG), 69.63 (PEG), 69.97 (PEG), 70.06 (PEG), 70.12−70.38 (m, PEG), 78.03 (*C*(CH$_3$)$_3$), 114.85 (dd, *C1*, ^1J(^{19}F−^{13}C) = 13.0 Hz, ^2J(^{19}F−^{13}C) = 5.5 Hz), 128.01 (dd, *C4*, ^1J(^{19}F−^{13}C) = 18.6 Hz, ^2J(^{19}F−^{13}C) = 14.2 Hz), 135.29 (d, *C2*, J(^{19}F−^{13}C) = 12.9 Hz), 137.18 (dm, *C5*, J(^{19}F−^{13}C) = 246.3 Hz), 144.48 (d, *C3*, J(^{19}F−^{13}C) = 254.6 Hz), 146.18 (C6, dm, J(^{19}F−^{13}C) = 251.8 Hz), 156.04 (COO), 168.39 (CON);

^{19}F NMR (376 MHz, DMSO-d_6): δ −125.00 (C3−*F*, s), −133.97 (C5−*F*, dd, ^1J = 26.9 Hz, ^2J = 12.6 Hz), −150.60 (C6−*F*, dd, ^1J = 27.0 Hz, ^2J = 6.6 Hz).

HRMS (m/z): [M]$^+$ calcd for $C_{46}H_{82}F_3N_4O_{18}S_2^+$, 1099.5013; found, 1099.5025.

4.6. General Procedure for the Syntheses of GZ21-10 and GZ22-3. **GZ21-9** (120.0 mg, 0.15 mmol, 1 equiv) or **GZ22-2** (130.0 mg, 0.12 mmol, 1 equiv) was dissolved in 1 mL of dichloromethane and added dropwise into trifluoracetic acid (4.5 g, 39.20 mmol, 260 equiv) precooled to 0 °C and then stirred at room temperature for 1 h. The reaction progress was monitored using TLC. The solvent was evaporated under reduced pressure, and the crude product was used for the next step without any additional purification.

4.7. *N*-(3-(2-(2-(3-Aminopropoxy)ethoxy)ethoxy)-propyl)-3-((2-(cyclooctylamino)-3,5,6-trifluoro-4-sulfamoylphenyl)sulfonyl)propanamide (GZ21-10). TLC (EtOAc): R_f = 0.1. Yield: 99.2 mg, 95%; yellow oily residue;

^{1}H NMR (400 MHz, DMSO-d_6): δ 1.47−1.75 (14H, m, cyclooctane (12H), PEG C*H*$_2$CH$_2$NH$_3$), 1.80−1.85 (4H, m, cyclooctane (2H), PEG NHCH$_2$C*H*$_2$), 2.64 (2H, t, J = 7.1 Hz, C*H*$_2$CONH), 2.89 (2H, s, J = 6.6 Hz, PEG C*H*$_2$NH$_3$), 3.08 (2H, q, J = 6.1 Hz, PEG CH$_2$CONHC*H*$_2$), 3.43 (2H, t, J = 6.3 Hz, C*H*$_2$CH$_2$CH$_2$NH$_3$), 3.49−3.60 (10H, m, OC*H*$_2$C*H*$_2$O (8H), NHCH$_2$CH$_2$C*H*$_2$), 3.80 (2H, t, J = 7.1 Hz, SO$_2$C*H*$_2$), 3.82−3.88 (1H, m, C*H* cyclooctane), 6.65 (1H, br s, N*H* cyclooctylamine), 8.15 (1H, t, J = 5.7, CH$_2$CON*H*), 8.39 (3H, s, N*H*$_3$), 8.42 (2H, s, N*H*$_2$SO$_2$).

^{19}F NMR (376 MHz, DMSO-d_6): δ −125.00 (C3−*F*, s), −133.93 (C5−*F*, dd, ^1J = 27.1 Hz, ^2J = 12.4 Hz), −150.58 (C6−*F*, dd, ^1J = 26.9 Hz, ^2J = 6.7 Hz).

HRMS (m/z): [M]$^+$ calcd for $C_{27}H_{46}F_3N_4O_8S_2^+$, 675.2704; found, 675.2703.

4.8. *N*-(35-Amino-3,6,9,12,15,18,21,24,27,30,33-undecaoxapentatriacontyl)-3-((2-(cyclooctylamino)-3,5,6-trifluoro-4-sulfamoylphenyl)sulfonyl)propanamide (GZ22-3). TLC (acetone/EtOAc/MeOH/CH_3COOH 33:33:33:1 v/v/v/v): R_f = 0.5. Yield: 118.1 mg, 94%; yellow oily residue;

HRMS (m/z): [M]$^+$ calcd for $C_{41}H_{74}F_3N_4O_{16}S_2^+$, 999.4488; found, 999.4483.

4.9. General Procedure for the Syntheses of GZ21-18 and GZ21-20. A solution of 2-(3-hydroxyphenyl)acetic acid (87.5 mg, 0.58 mmol, 10 equiv) or 3-(4-hydroxyphenyl)-propanoic acid (77.0 mg, 0.47 mmol, 10 equiv for **GZ21-20**) was mixed with 2 mL of water, and 0.41 mL of 1 M Na_2CO_3 was added dropwise into the mixture until pH 10. Then, NIR-783 (50.0 mg, 0.07 mmol, 1 equiv or 35.0 mg, 0.05 mmol, 1 equiv for **GZ21-20**) was added, and the mixture was stirred at 70 °C for 24 h. The reaction progress was monitored using TLC. The solvent was evaporated under reduced pressure, and the residue was purified with column chromatography.

4.10. Sodium 4-((*Z*)-2-((*E*)-2-(2-(3-(Carboxymethyl)-phenoxy)-3-((*E*)-2-(3,3-dimethyl-1-(4-sulfonatobutyl)-3*H*-indol-1-ium-2-yl)vinyl)cyclohex-2-en-1-ylidene)-ethylidene)-3,3-dimethylindolin-1-yl)butane-1-sulfonate (GZ21-18). TLC (MeOH/acetone/$CHCl_3$, 1:1:1 v/v/

https://doi.org/10.1021/acs.bioconjchem.4c00144
Bioconjugate Chem. 2024, 35, 790−803

v): R_f = 0.5. Purified with column chromatography (gradient: MeOH/acetone/EtOAc, 1:1:1 v/v/v → MeOH). Yield: 62.0 mg, 78%; mp 226−228 °C;

^{1}H NMR (400 MHz, DMSO-d_6): δ 1.29 (12H, s, CH_3), 1.65−1.81 (8H, m, $NCH_2CH_2CH_2$), 1.89−1.97 (2H, m, $OCCCH_2CH_2$), 2.44−2.54 (4H, m (inside DMSO peak), $OCCCH_2$), 2.72 (4H, t, J = 6.0 Hz, SO_3CH_2), 3.33 (2H, s, CH_2COOH), 4.12 (4H, t, J = 7.2 Hz, NCH_2), 6.21 (2H, d, J = 14.2 Hz, OCCC*H*), 6.84 (1H, dd, J = 8.0, 2.6 Hz, OCC*H*CH), 6.96 (1H, d, J = 7.5 Hz, OCCHCHC*H*), 7.13 (1H, s, OCC*H*C), 7.15−7.25 (3H, m, indolene), 7.31−7.42 (4H, m, indolene), 7.50 (2H, d, J = 7.4 Hz, OCCHC*H*CH), 7.86 (2H, d, J = 14.1 Hz, OCCCHC*H*), acid peak inside H_2O.

^{13}C NMR (100 MHz, DMSO-d_6): δ 22.99, 23,94, 24.25, 26.47, 27.71, 40.84, 43.98, 45.57, 49.01, 51.17, 100.63, 111.55, 111.68, 116.07, 122.20, 122.80, 123.96, 125.07, 128.88, 129.79, 141.54, 142.55, 159.67, 163.61, 171.93, 174.20, 174.42.

HRMS (m/z): $[M]^-$ calcd for $C_{46}H_{53}N_9O_{10}S_2^-$, 841.3197; found, 841.3114.

4.11. Sodium 4-((*Z*)-2-((*E*)-2-(2-(4-(2-Carboxyethyl)-phenoxy)-3-((*E*)-2-(3,3-dimethyl-1-(4-sulfonatobutyl)-3*H*-indol-1-ium-2-yl)vinyl)cyclohex-2-en-1-ylidene)-ethylidene)-3,3-dimethylindolin-1-yl)butane-1-sulfonate (GZ21-20). TLC (MeOH/acetone/EtOAc, 1:1:1 v/v/v): R_f = 0.1. Purified with column chromatography (gradient: MeOH/acetone/EtOAc, 1:1:1 v/v/v → MeOH). Yield: 37.0 mg, 90%; mp 225−228 °C;

^{1}H NMR (400 MHz, DMSO-d_6): δ 1.25 (12H, s, CH_3), 1.62−1.79 (8H, m, $NCH_2CH_2CH_2$), 1.88−1.97 (2H, m, $OCCCH_2CH_2$), 2.10 (2H, t, J = 7.8 Hz, CH_2CH_2COOH), 2.36−2.56 (4H, m (inside DMSO peak), $OCCCH_2$), 2.63−2.77 (6H, m, CH_2COOH and SO_3CH_2), 4.12 (4H, t, J = 7.8 Hz, NCH_2), 6.21 (2H, d, J = 14.2 Hz, OCCC*H*), 7.02 (2H, d, J = 8.5 Hz, OCC*H*), 7.14−7.24 (4H, m, indolene), 7.31−7.41 (4H, m, indolene), 7.49 (2H, d, J = 7.4 Hz, OCCHC*H*), 7.82 (2H, d, J = 14.1 Hz, OCCCHC*H*), acid peak inside H_2O.

^{13}C NMR (100 MHz, DMSO-d_6): δ 22.99, 24.18, 24.98, 26.48, 27.67, 31.94, 43.96, 48.96, 49.04, 51.17, 100.65, 111.66, 114.56, 122.04, 122.82, 125.12, 126.73, 128.94, 130.37, 137.42, 141.41, 142.54, 158.15, 163.22, 171.86, 175.83.

HRMS (m/z): $[M]^-$ calcd for $C_{47}H_{55}N_2O_9S_2^-$, 855.3354; found, 855.3327.

4.12. Sodium 4-((*Z*)-2-((*E*)-2-(2-(3-(20-((2-(Cyclooctylamino)-3,5,6-trifluoro-4-sulfamoylphenyl)sulfonyl)-2,18-dioxo-7,10,13-trioxa-3,17-diazaicosyl)phenoxy)-3-((*E*)-2-(3,3-dimethyl-1-(4-sulfonatobutyl)-3*H*-indol-1-ium-2-yl)vinyl)cyclohex-2-en-1-ylidene)ethylidene)-3,3-dimethylindolin-1-yl)butane-1-sulfonate (GZ21-19). A mixture of **GZ21-18** (18.0 mg, 20.8 μmol, 1 equiv), **GZ21-10** (15.0 mg, 22.8 μmol, 1.1 equiv), EDC (10.7 mg, 62.4 μmol, 3 equiv), HOBT (6.0 mg, 41.6 μmol, 2 equiv), 0.5 mL of dry pyridine, and 3 mL of DMSO was stirred at room temperature under an argon atmosphere for 48 h. The reaction progress was monitored using TLC (EtOAc/acetone/MeOH, 2:2:3 v/v/v): R_f = 0.7. The solvent was evaporated under reduced pressure, then the crude product was poured into saturated sodium chloride solution (10 mL), acidified until neutral pH, and extracted with ethyl acetate. The organic layer was washed with sat. sodium chloride solution and dried over sodium sulfate. The solvent was evaporated under reduced pressure, and the residue was purified with column chromatography (MeOH/EtOAc/acetone, 1:1:1 v/v/v). Yield: 2.0 mg, 6%;

^{1}H NMR (400 MHz, DMSO-d_6): δ 1.25 (12H, s, CH_3), 1.38−1.91 (28H, m, (4H $NCH_2CH_2CH_2$, 2H $OCCCH_2CH_2$, 8H $SO_3CH_2CH_2CH_2$ and 14H cyclooctane)), 2.37−2.72 (6H, m, SCH_2CH_2CONH and $OCCCH_2$ (overlapping DMSO residual peak)), 2.66−2.76 (4H, m, SO_3CH_2), 2.92−3.11 (6H, m, PEG CH_2NH and CCH_2CON), 3.20−3.97 (15H, m, SO_2CH_2, C*H* cyclooctane and PEG), 4.12 (4H, s, NCH_2), 6.22 (2H, d, J = 14.2 Hz, OCCC*H*), 6.55−6.65 (1H, m, N*H* cyclooctylamine), 6.89−7.55 (12H, m, phenol, indolene), 7.81 (2H, d, J = 14.6 Hz, OCCCHC*H*), 8.04−8.24 (2H, m, N*H*CO).

^{19}F NMR (376 MHz, DMSO-d_6): δ −125.00 (C3−*F*, s), −133.97 (C5−*F*, d, J = 27.1 Hz), −150.58 (C6−*F*, d, J = 24.1 Hz).

HRMS (m/z): $[M]^+$ calcd for $C_{73}H_{98}F_3N_4O_{16}S_4^+$, 1499.5869; found, 1499.5870.

4.13. General Procedure for the Syntheses of GZ22-1 and GZ22-4. A mixture of **GZ21-20** (20.0 mg, 22.7 μmol, 1 equiv), **GZ21-10** (16.9 mg, 25.0 μmol, 1.1 equiv) or **GZ22−3** (25.0 mg, 25.0 μmol, 1.1 equiv) for **GZ22-4**, EDC (8.8 mg, 56.8 μmol, 2.5 equiv), HOBT (6.1 mg, 45.5 μmol, 2 equiv), 0.5 mL of dry pyridine, and 3 mL of DMF was stirred at room temperature under an argon atmosphere for 24 h. The reaction progress was monitored using TLC. The solvent was evaporated under reduced pressure, and the crude product was poured into saturated sodium chloride solution (10 mL), acidified until neutral pH, and extracted with ethyl acetate. The organic layer was washed with sat. sodium chloride solution and dried over sodium sulfate. The solvent was evaporated under reduced pressure and residue was purified with column chromatography.

4.14. Sodium 4-((*Z*)-2-((*E*)-2-(2-(4-(21-((2-(Cyclooctylamino)-3,5,6-trifluoro-4-sulfamoylphenyl)sulfonyl)-3,19-dioxo-8,11,14-trioxa-4,18-diazahenicosyl)phenoxy)-3-((*E*)-2-(3,3-dimethyl-1-(4-sulfonatobutyl)-3*H*-indol-1-ium-2-yl)vinyl)cyclohex-2-en-1-ylidene)ethylidene)-3,3-dimethylindolin-1-yl)butane-1-sulfonate (GZ22-1). TLC (acetone/MeOH/EtOAc, 1:1:1 v/v/v): R_f = 0.4. Purified with column chromatography (acetone/MeOH/EtOAc, 1:1:1 v/v/v). Yield: 5.1 mg, 15%;

^{1}H NMR (400 MHz, DMSO-d_6): δ 1.31 (12H, s, CH_3), 1.44−0.04 (28H, m, $NCH_2CH_2CH_2$ (4H), $OCCCH_2CH_2$, $SO_3CH_2CH_2CH_2$ (8H) and cyclooctane (14H)), 2.27−2.35 (2H, m, CCH_2CH_2CO), 2.49−2.60 (4H, m, $OCCCH_2$ (overlapping DMSO residual peak)), 2.65 (2H, t, J = 6.8 Hz, SCH_2CH_2CONH), 2.71−2.82 (4H, m, SO_3CH_2), 3.01−3.11 (4H, m, PEG CH_2NH), 3.32−4.12 (17H, m, SO_2CH_2, CCH_2CON, C*H* cyclooctane and PEG), 4.14−4.22 (4H, s, NCH_2), 6.27 (2H, d, J = 14.2 Hz, OCCC*H*), 6.64 (1H, d, J = 8.8 Hz, N*H* cyclooctylamine), 7.06−7.13 (2H, m, phenol), 7.20−7.33 (4H, m, indolene), 7.36−7.46 (4H, m, indolene), 7.54 (2H, d, J = 7.5 Hz, phenol), 7.87 (2H, d, J = 14.0 Hz, OCCCHC*H*), 7.98 (1H, t, J = 5.7 Hz, SCH_2CH_2CONH), 8.20−8.31 (1H, m, $NHCOCH_2CH_2C$).

^{19}F NMR (376 MHz, DMSO-d_6): δ −125.00 (C3−*F*, s), −133.97 (C5−*F*, d, J = 27.1 Hz), −150.58 (C6−*F*, d, J = 24.1 Hz).

HRMS (m/z): $[M]^-$ calcd for $C_{74}H_{98}F_3N_6O_{16}S_4^-$, 1511.5879; found, 1511.5818.

4.15. Sodium 4-((*Z*)-2-((*E*)-2-(2-(4-(43-((2-(Cyclooctylamino)-3,5,6-trifluoro-4-sulfamoylphenyl)sulfonyl)-3,41-dioxo-7,10,13,16,19,22,25,28,31,34,37-undecaoxa-4,40-diazatritetracontyl)phenoxy)-3-((*E*)-2-(3,3-dimethyl-1-

https://doi.org/10.1021/acs.bioconjchem.4c00144
Bioconjugate Chem. 2024, 35, 790−803

(4-sulfonatobutyl)-3*H*-indol-1-ium-2-yl)vinyl)cyclohex-2-en-1-ylidene)ethylidene)-3,3-dimethylindolin-1-yl)-butane-1-sulfonate (GZ22-4). TLC (acetone/MeOH/AcOH, 33:66:1 v/v/v): R_f = 0.3. Purified with column chromatography (MeOH/acetone, 1:3 v/v). Yield: 4.0 mg, 9%

^{1}H NMR (400 MHz, DMSO-d_6): δ 1.26 (12H, s, CH_3), 1.39−1.88 (22H, m, (8H $NCH_2CH_2CH_2$ and 14H cyclooctane)), 1.89−1.98 (2H, m, $OCCCH_2CH_2$), 2.27 (2H, t, J = 8.0 Hz, CCH_2CH_2CON), 2.42−2.54 (4H, m (overlapping DMSO residual peak), $OCCCH_2$), 2.60 (2H, t, J = 7.1 Hz, SCH_2CH_2CONH), 2.65−2.77 (6H, m, CCH_2CH_2CON and SO_3CH_2), 3.08−3.17 (4H, m, PEG CH_2NH), 3.49 (44H, s, PEG), 3.73 (2H, t, J = 7.1 Hz, SO_2CH_2), 3.75−3.82 (1H, m, C*H* cyclooctane), 4.13 (4H, t, J = 7.2 Hz, NCH_2), 6.22 (2H, d, J = 14.2 Hz, OCCC*H*), 6.59 (1H, d, J = 7.9 Hz, N*H* cyclooctylamine), 7.06 (2H, d, J = 8.1 Hz, OCC*H*), 7.15−7.24 (4H, m, indolene), 7.32−7.42 (4H, m, indolene), 7.48 (2H, d, J = 7.5 Hz, OCCHC*H*), 7.82 (2H, d, J = 13.9 Hz, OCCCHC*H*), 7.83−7.88 (1H, m, $NHCOCH_2CH_2C$), 8.15 (1H, t, J = 5.3, $SO_2CH_2CH_2CONH$).

^{19}F NMR (376 MHz, DMSO-d_6): δ −125.02 (C3−*F*, s), −134.05 (C5−*F*, dd, ^1J = 27.2 Hz, ^2J = 12.5 Hz), −150.56 (C6−*F*, dd, ^1J = 27.1 Hz, ^2J = 6.4 Hz).

HRMS (m/z): $[M]^+$ calcd for $C_{88}H_{128}F_3N_6O_{24}S_4^+$, 1837.7810; found, 1837.7844.

4.16. *tert*-Butyl (1-((2-(Cyclooctylamino)-3,5,6-trifluoro-4-sulfamoylphenyl)sulfonyl)-4,7-dioxo-12,15,18-trioxa-3,8-diazahenicosan-21-yl)carbamate (AZ21-4). Commercially available 2,2-dimethyl-4,20-dioxo-3,9,12,15-tetraoxa-5,19-diazatricosan-23-oic acid (93 mg, 0.22 mmol) was dissolved in DMF (2 mL) and pyridine (1 mL), then EDC (58 mg, 0.30 mmol) was added, and the reaction mixture was stirred for 1 h at room temperature, under an argon atmosphere. Then, 4-((2-aminoethyl)sulfonyl)-3-(cyclooctylamino)-2,5,6-trifluorobenzenesulfonamide hydrochloride (AZ21-1B) (114 mg, 0.24 mmol) was added, and the reaction mixture was stirred for 24 h at room temperature, under an argon atmosphere. The solvents were removed at reduced pressure, and the resultant precipitate was dissolved in ethyl acetate. The organic extract was washed with 5% HCl(aq), then with 5% $NaHCO_3$, and dried over sodium sulfate. The solvent was evaporated under reduced pressure, and the residue was purified with column chromatography (ethyl acetate/MeOH (5:1), R_f = 0.7). Yield: 116.0 mg, 62%, yellow oily residue.

^{1}H NMR (400 MHz, DMSO-d_6): δ 1.37 (9H, s, $C(CH_3)_3$), 1.42−1.68 (16H, m, cyclooctane (12H) and $OCH_2CH_2CH_2NH$ (4H)), 1.81−1.88 (2H, m, cyclooctane), 2.18−2.27 (4H, $HNCOCH_2CH_2CONH$), 2.96 (2H, q, J = 6.4 Hz, $CONHCH_2CH_2CH_2O$), 3.06 (2H, q, J = 6.4 Hz, $CONHCH_2CH_2CH_2O$), 3.38 (4H, t, J = 6.0 Hz, $NHCH_2CH_2CH_2O$), 3.41−3.53 (10H, m, OCH_2CH_2O (8H) and $CONHCH_2CH_2SO_2$), 3.68 (2H, t, J = 6.4 Hz, SO_2CH_2), 3.77 (1H, br s, C*H* cyclooctane), 6.60 (1H, d, J = 8.0 Hz, N*H*-cyclooctyl), 6.76 (1H, t, J = 5.6 Hz, N*H*COO), 7.79 (1H, t, J = 5.6 Hz, N*H*CO), 8.06 (1H, t, J = 5.2 Hz, CON*H*$CH_2CH_2SO_2$), 8.36 (2H, s, SO_2NH_2).

^{19}F NMR (376 MHz, DMSO-d_6): δ −124.7 (C2−*F*, s), −134.4 (C6−*F*, dd, ^1J = 26.9 Hz, ^2J = 12.9 Hz), −150.2 (C5−*F*, dd, ^1J = 27.0 Hz, ^2J = 6.4 Hz).

HRMS for $C_{35}H_{58}F_3N_5O_{11}S_2$ $[(M + H)^+]$: calcd, 846.3599; found, 846.3613.

4.17. Sodium 4-((*Z*)-2-((*E*)-2-(2-((1-((2-(Cyclooctylamino)-3,5,6-trifluoro-4-sulfamoylphenyl)sulfonyl)-4,7-dioxo-12,15,18-trioxa-3,8-diazahenicosan-21-yl)-amino)-3-((*E*)-2-(3,3-dimethyl-1-(4-sulfonatobutyl)-3*H*-indol-1-ium-2-yl)vinyl)cyclohex-2-en-1-ylidene)-ethylidene)-3,3-dimethylindolin-1-yl)butane-1-sulfonate (AZ21-6). **AZ21-4** (32 mg, 0.038 mmol) was dissolved in dichloromethane (7 mL) and TFA (0.3 mL), and the reaction mixture was stirred for 2 h at room temperature. The solvents were removed at reduced pressure, and the resultant precipitate was dissolved in DMF (3 mL). Then, NIR-783 (33 mg, 0.044 mmol) and DIPEA (50 μL, 0.287 mmol) were added, and the reaction mixture was stirred for 24 h at room temperature under an argon atmosphere. The solvents were removed at reduced pressure, and the residue was purified with column chromatography (chloroform/ethyl acetate/MeOH (1:1:1), R_f = 0.37). Yield: 27 mg, 49%.

^{1}H NMR (400 MHz, DMSO-d_6): δ 1.42−1.77 (34H, m, $C(CH_3)_2$ (12H), cyclooctane (12H), CH_2(IR-dye) (6H) and $OCH_2CH_2CH_2NH$ (4H)), 1.79−1.88 (6H, m, cyclooctane (2H) and CH_2(IR-dye) (4H), 2.16−2.26 (4H, $HNCOCH_2CH_2CONH$), 2.48 (4H, m, CH_2(IR-dye) overlapping with DMSO), 3.02 (4H, m, $NHCH_2CH_2CH_2O$), 3.30−3.55 (14H, m, $NHCH_2CH_2CH_2O$ (4H), $(OCH_2CH_2O)_2$ and $CONHCH_2CH_2SO_2$, overlapping with H_2O), 3.63−3.70 (2H, m, SO_2CH_2), 3.76 (1H, br s, C*H* cyclooctane), 3.83−3.94 (4H, m, CH_2SO_3), 5.71 (2H, d, J = 8.4 Hz, NHCCC*H*), 6.57 (1H, d, J = 8.0 Hz, N*H*-cyclooctyl), 7.00 (2H, t, J = 7.6 Hz, indolene),7.09 (2H, d, J = 8.4 Hz, indolene), 7.25 (2H, t, J = 7.6 Hz, indolene), 7.39 (2H, d, J = 7.6 Hz, indolene), 7.47 (2H, d, J = 9.6 Hz, NHCCCHC*H*), 7.85 (1H, s, N*H*CO), 8.09 (1H, s, CON*H*$CH_2CH_2SO_2$).

^{19}F NMR (376 MHz, DMSO-d_6): δ −124.8 (C2−*F*, s), −134.7 (C6−*F*, d, J = 24.1 Hz), −150.4 (C5−*F*, d, J = 25.6 Hz).

HRMS for $C_{68}H_{95}F_3N_7O_{15}S_4$ $[(M\text{-}H)^-]$: calcd, 1434.5727; found, 1434.5660.

4.18. Preparation of Recombinant CA Isozymes. All 12 catalytically active human CA isozymes were prepared recombinantly as previously described. Most isozymes were truncated, and only the catalytic domains of the proteins were produced.[9,56] All isozymes were expressed in a bacterial expression system except that CAIX was expressed in mammalian cells. The proteins were chromatographically purified via immobilized metal affinity chromatography, ion-exchange, or *p*-aminomethylbenzenesulfonamide-sepharose affinity chromatography. Protein purity was confirmed by SDS-PAGE, and MW was confirmed by mass spectrometry with 1 Da precision, as predicted from theoretical protein sequence.

4.19. Fluorescence-Based Thermal Shift Assay. The fluorescence-based thermal shift assay (FTSA) was used to determine the binding affinity of compounds for all catalytically active CA isozymes. The assay is based on the thermal stabilization of proteins by bound ligands and distinguishes itself in its ability to determine extremely high affinity (picomolar K_d) of compound binding to CAIX. The experiments were performed with a QIAGEN Rotor-Gene Q instrument using either the blue channel (365 ± 20 nm excitation and 460 ± 15 nm emission detection) or the green channel (470 ± 10 nm excitation and 510 ± 5 nm detection). The protein solution, in the absence and presence of various compound concentrations ranging from 3 to 200 μM (2×

https://doi.org/10.1021/acs.bioconjchem.4c00144
Bioconjugate Chem. 2024, 35, 790−803

dilutions), was heated from 25 to 99 °C (heating rate, 1 °C/min). The CA isozyme melting temperature T_m was determined by following the fluorescence of 8-anilino-1-naphthalenesulfonate (ANS) or Glomelt dye. The samples consisted of 5 μM protein (or 10 μM CAIV), different concentrations of the tested compound, and 50 μM ANS or 200× diluted Glomelt in 50 mM sodium phosphate buffer (at pH 7.0) containing 100 mM sodium chloride and 2−4% (v/v) dimethyl sulfoxide. To obtain the dissociation constant (at 37 °C), data analysis was performed, and the curves were fit using the Thermott Web server.[57]

4.20. Construction of the CAIX Expression Plasmid. The cDNA of human carbonic anhydrase IX (CAIX) in pOTB7 vector was purchased from RZPD Deutsches Ressourcenzentrum für Genomforschung GmbH (Germany). For the construction of the mammalian CAIX expression plasmid pCMV-CAIX, the cDNA fragment, encoding full-length CAIX sequence, was cut out from the pOTB7-CAIX plasmid using restriction endonucleases PsiI and Ppu21I (partial digestion) and inserted into the pCMV-HA vector (Clontech) via digested ApaI and XhoI restriction sites, blunted by Klenow fragment. The pCMV-CAIX expression plasmid contains an open reading frame for the full-length CAIX protein (1−459 amino acids) without a tag because the HA tag, originally present in the pCMV-HA vector, was removed during the subcloning procedure.

4.21. Measurement of Compound Binding to Live Cells and Compound Competition Assay. Both assays were performed as previously described.[16] In brief, to measure fluorescent compound binding to CAIX expressed in live cells, HeLa cells were seeded in 12-well plates and either incubated in hypoxia for 3 days or transfected with the CAIX-coding plasmid pCMV-CAIX next day after seeding. The TurboFect transfection reagent (Thermo Fisher) was used for transfection. After 3 days in hypoxia or next day after transfection in normoxia, the cell medium from each well was removed and replaced by 200 μL of a serially diluted NIR-fluorescent compound (12 2-fold dilution steps) in the PBS medium, starting from 4 μM (4, 2, 1,..., 0 nM). Plates were incubated in a CO_2 incubator at normoxia for 20 min. The solution was removed, and cells were washed 3 times for 1−2 min with 400 μL of PBS. Then, 180 μL of TrypLe express enzyme (Thermo Fisher) was added to each well. After 10 min at normoxia, 20 μL of Defined Trypsin Inhibitor solution (Thermo Fisher) was added and cells were resuspended by pipetting. 150 μL of the suspension from each well was transferred to Thermo Scientific Nunc MicroWell 96-Well Optical-Bottom Plates for fluorescence and absorbance measurements. 759 nm excitation and 800 nm emission wavelengths were used to measure fluorescence on a Synergy HTX, BioTek plate reader. 650 nm wavelength was used for absorbance measurements.

For the competition assay, live cells were seeded in 12-well plates and incubated for 3 days under hypoxia. 200 μL of serially diluted NIR-fluorescent compound (12 2-fold dilution steps) in the PBS medium, starting from 5120 nM (5120, 2560, 1280,..., 0 nM), was mixed with 200 μL of 20 nM **GZ19-32** solution (PBS). After the removal of growth medium, 200 μL obtained solutions were applied to the cells grown in 12-well culture plates. Plates were incubated in the CO_2 incubator at normoxia for 20 min. The solution was removed, and cells were washed 3 times for 1−2 min with 400 μL of PBS. Then, 180 μL of TrypLe express enzyme (Thermo Fisher) was added to each well and incubated in the normoxia chamber for 10 min. Then, 20 μL of Defined Trypsin Inhibitor solution (Thermo Fisher) was added and cells were resuspended by pipetting. 150 μL of the suspension from each well was transferred to Thermo Scientific Nunc MicroWell 96-Well Optical-Bottom Plates for fluorescence and absorbance measurements. 485 nm excitation and 520 nm emission wavelengths were used to measure fluorescence on a Synergy HTX, BioTek plate reader. 650 nm wavelength was used for absorbance measurements.

4.22. Cell Culture and Staining of Live Cells. Human cervical adenocarcinoma cells (HeLa) were kindly provided by Dr. A. Kanopka (Vilnius University). The CAIX-knockout cell line ($HeLaCAIX^{KO}$) was developed using the CRISPR-Cas9 knockout system as described previously.[16] HeLa cells were cultured in Dulbecco's modified Eagle's medium (DMEM) with GlutaMAX (Gibco, Thermo Fisher), supplemented with 10% of heat-inactivated fetal bovine serum, 100 units/mL penicillin, and 100 mg/mL streptomycin in a humidified atmosphere at 37 °C and 5% CO_2. Hypoxia, when needed, was achieved in the humidified CO_2 incubator with oxygen control (Binder, Germany), using conditions of 1% O_2, 5% CO_2, and 94% N_2 and 37 °C. Cells were regularly checked for mycoplasma contamination using a SouthernBiotech Mycoplasma Detection Kit (#OB1310001) according to manufacturer's directions.

For visualization of CAIX in live cells, HeLa cells were seeded in 12-well plates, and the next day they were transfected with the pCMV-CAIX plasmid to induce CAIX expression under normoxia. The TurboFect Transfection Reagent (Thermo Fisher) was used for this purpose according to manufacturer's directions. Cells were stained and visualized next day after transfection. Nontransfected cells, grown under normoxia, were used as a control. For the induction of CAIX expression without transfection, cells were cultured under hypoxia for 3 days.

For cell imaging, live cells were incubated with the recombinant monoclonal antibody to CAIX (M75) (Absolute Antibody, #Ab00414−1.1) in the CO_2 incubator for 30 min. The antibody stock solution (1 mg/mL) was used at a dilution of 1:150 in FluoroBright (FB)(Thermo Fisher) medium. After washing (3 × 5 min with DMEM in RT, gentle rock), cells were incubated with secondary Alexa Fluor 488 goat antimouse antibodies (2 mg/mL, Thermo Fisher), at a dilution of 1:200 in FB, in a CO_2 incubator for 30 min. After washing (3 × 5 min with DMEM in RT and 2 × 1 min with PBS), cells were incubated with NIR-fluorescent inhibitors (250 nm in PBS) in a CO_2 incubator for 5−8 min. After washing (2 min + 2 × 1 min with PBS), PBS was replaced by FB, and 15 μL of NucBlue Live Cell Stain ReadyProbes reagent (Thermo Fisher) was added per well. After 5 min, cells were observed and photographed using an automated fluorescence microscope EVOS FL Auto (Thermo Fisher).

4.23. Mice. Female nude mice (CR ATH HO Code 24106216), 5−6 weeks old, were obtained from Charles River Laboratories. Animals were housed, bred, and handled in the Department of Animal Models Animal Facility at the Life Sciences Center, Vilnius University, Lithuania, with a 12 h light−dark cycle, at 21−23 °C and 40−60% humidity. Animals were fed with an irradiated cholorophyll-deficient diet (Altromin, #C1086194) and water ad libitum. All experimental procedures conformed to Directive 2010/63/EU requirements

https://doi.org/10.1021/acs.bioconjchem.4c00144
Bioconjugate Chem. 2024, 35, 790−803

and were approved by the Lithuanian State Food and Veterinary Service (Approval no G2-194, 2021-11-09).

Before injection into animals, mycoplasma-free cells in the exponential growth phase were harvested, washed, and resuspended in PBS. 8−12 weeks old female nude mice were inoculated S.Q. with 3×10^6 HeLaCAIX^{WT} cells in 100 μL of PBS into the right flank of the mice, and the same number of HeLaCAIX^{KO} cells were injected into the left flank of the same mouse. Once tumors reached a suitable size for imaging, **GZ22-4** or **AZ21-6** compounds were injected I.V. at a dose of 2 mg/kg/dose once. Mice were imaged every 24 h post-injection using isoflurane anesthesia with an Alliance^{TM} ^{b}Q9 Imager system. Images were quantified using the UVIBAND MAX analysis software system. At the end of the experiment, animals were euthanized with a flow of 8.0 L/min of medical CO_2 gas (Elme Messer Lit, Vilnius, Lithuania) followed by cervical dislocation.

■ ASSOCIATED CONTENT

Supporting Information

The Supporting Information is available free of charge at https://pubs.acs.org/doi/10.1021/acs.bioconjchem.4c00144.

Information on NIR inhibitor absorption and emission spectra, microphotographs of cells stained with **GZ22-1** and **GZ21-19** compounds, comparison at identical exposure conditions, NIR fluorescent inhibitor quantum yields, and ^{1}H and ^{19}F NMR spectra of **GZ22-4** compound (PDF)

■ AUTHOR INFORMATION

Corresponding Author

Daumantas Matulis − *Department of Biothermodynamics and Drug Design, Institute of Biotechnology, Life Sciences Center, Vilnius University, Vilnius LT-10257, Lithuania;* orcid.org/0000-0002-6178-6276; Email: daumantas.matulis@bti.vu.lt, matulis@ibt.lt

Authors

Gediminas Žvinys − *Department of Biothermodynamics and Drug Design, Institute of Biotechnology, Life Sciences Center, Vilnius University, Vilnius LT-10257, Lithuania*

Agne Petrosiute − *Department of Biothermodynamics and Drug Design, Institute of Biotechnology, Life Sciences Center, Vilnius University, Vilnius LT-10257, Lithuania*

Audrius Zakšauskas − *Department of Biothermodynamics and Drug Design, Institute of Biotechnology, Life Sciences Center, Vilnius University, Vilnius LT-10257, Lithuania*

Asta Zubrienė − *Department of Biothermodynamics and Drug Design, Institute of Biotechnology, Life Sciences Center, Vilnius University, Vilnius LT-10257, Lithuania*

Alvilė Ščerbavičienė − *Department of Biological Models, Institute of Biochemistry, Life Sciences Center, Vilnius University, Vilnius LT-10257, Lithuania*

Zane Kalnina − *Latvian Biomedical Research and Study Centre, Riga LV-1067, Latvia*

Edita Čapkauskaitė − *Department of Biothermodynamics and Drug Design, Institute of Biotechnology, Life Sciences Center, Vilnius University, Vilnius LT-10257, Lithuania*

Vaida Juozapaitienė − *Department of Biothermodynamics and Drug Design, Institute of Biotechnology, Life Sciences Center, Vilnius University, Vilnius LT-10257, Lithuania*

Aurelija Mickevičiūtė − *Department of Biothermodynamics and Drug Design, Institute of Biotechnology, Life Sciences Center, Vilnius University, Vilnius LT-10257, Lithuania*

Kirill Shubin − *Latvian Institute of Organic Synthesis, Riga LV-1006, Latvia*

Švitrigailė Grincevičienė − *Department of Biothermodynamics and Drug Design, Institute of Biotechnology, Life Sciences Center, Vilnius University, Vilnius LT-10257, Lithuania*

Steponas Raišys − *Institute of Photonics and Nanotechnology, National Center for Physical Sciences and Technology, Vilnius University, Vilnius LT-10257, Lithuania;* orcid.org/0000-0002-5810-7199

Kaspars Tars − *Latvian Biomedical Research and Study Centre, Riga LV-1067, Latvia;* orcid.org/0000-0001-8421-9023

Jurgita Matulienė − *Department of Biothermodynamics and Drug Design, Institute of Biotechnology, Life Sciences Center, Vilnius University, Vilnius LT-10257, Lithuania*

Complete contact information is available at: https://pubs.acs.org/10.1021/acs.bioconjchem.4c00144

Notes

The authors declare the following competing financial interest(s): The authors declare that they have patents and patent applications pending on carbonic anhydrase inhibitors.

■ ACKNOWLEDGMENTS

This study was funded by the Research Council of Lithuania, Healthy Ageing program project S-SEN-20-10.

■ ABBREVIATIONS

CA, carbonic anhydrase; CAIX, carbonic anhydrase isozyme IX; DCM, dichloromethane; DIPEA, diisopropylethylamine; DMF, dimethylformamide; DMSO, dimethyl sulfoxide; EDC, 1-ethyl-3-(3-(dimethylamino)propyl)carbodiimide; FTSA, fluorescence-based thermal shift assay; HeLa, human cervical adenocarcinoma cells; HOBt, hydroxybenzotriazole; IR, infrared; KO, knock out; NMR, nuclear magnetic resonance; PEG, polyethylene glycol; Py, pyridine; TFA, trifluoroacetic acid; TLC, thin-layer chromatography; TMS, tetramethylsilane; TSA, thermal shift assay; WT, wild type

■ REFERENCES

(1) Bai, J.-W.; Qiu, S.-Q.; Zhang, G.-J. Molecular and Functional Imaging in Cancer-Targeted Therapy: Current Applications and Future Directions. *Signal Transduction Targeted Ther.* **2023**, *8* (1), 89.

(2) Tafreshi, N. K.; Lloyd, M. C.; Bui, M. M.; Gillies, R. J.; Morse, D. L. Carbonic Anhydrase IX as an Imaging and Therapeutic Target for Tumors and Metastases. *Subcell. Biochem.* **2014**, *75*, 221−254.

(3) Gardeen, S.; Low, P. S. Use of Carbonic Anhydrase IX Inhibitors for Selective Delivery of Attached Drugs to Solid Tumors. In *Carbonic Anhydrase as Drug Target* Matulis, D., Ed.; Springer International Publishing: Cham, 2019; pp 289−303..

(4) Sun, J.; Huangfu, Z.; Yang, J.; Wang, G.; Hu, K.; Gao, M.; Zhong, Z. Imaging-Guided Targeted Radionuclide Tumor Therapy: From Concept to Clinical Translation. *Adv. Drug Delivery Rev.* **2022**, *190*, 114538.

(5) Chen, K.-T.; Seimbille, Y. New Developments in Carbonic Anhydrase IX-Targeted Fluorescence and Nuclear Imaging Agents. *Int. J. Mol. Sci.* **2022**, *23* (11), 6125.

(6) Stillebroer, A. B.; Zegers, C. M. L.; Boerman, O. C.; Oosterwijk, E.; Mulders, P. F. A.; O'Donoghue, J. A.; Visser, E. P.; Oyen, W. J. G. Dosimetric Analysis of 177Lu-cG250 Radioimmunotherapy in Renal

Cell Carcinoma Patients: Correlation with Myelotoxicity and Pretherapeutic Absorbed Dose Predictions Based on 111In-cG250 Imaging. *J. Nucl. Med.* **2012**, *53* (1), 82−89.
(7) Kulterer, O. C.; Pfaff, S.; Wadsak, W.; Garstka, N.; Remzi, M.; Vraka, C.; Nics, L.; Mitterhauser, M.; Bootz, F.; Cazzamalli, S.; Krall, N.; Neri, D.; Haug, A. R. A Microdosing Study with 99mTc-PHC-102 for the SPECT/CT Imaging of Primary and Metastatic Lesions in Renal Cell Carcinoma Patients. *J. Nucl. Med.* **2021**, *62* (3), 360−365.
(8) Zhu, W.; Li, X.; Zheng, G.; Bai, C.; Ji, Z.; Zhang, H.; Xing, H.; Zhang, Y.; Huo, L. Preclinical and Pilot Clinical Evaluation of a Small-Molecule Carbonic Anhydrase IX Targeting PET Tracer in Clear Cell Renal Cell Carcinoma. *Eur. J. Nucl. Med. Mol. Imaging* **2023**, *50* (10), 3116−3125.
(9) Dudutienė, V.; Matulienė, J.; Smirnov, A.; Timm, D. D.; Zubrienė, A.; Baranauskienė, L.; Morkūnaitė, V.; Smirnovienė, J.; Michailovienė, V.; Juozapaitienė, V.; Mickevičiūtė, A.; Kazokaitė, J.; Bakšytė, S.; Kasiliauskaitė, A.; Jachno, J.; Revuckienė, J.; Kišonaitė, M.; Pilipuitytė, V.; Ivanauskaitė, E.; Milinavičiūtė, G.; Smirnovas, V.; Petrikaitė, V.; Kairys, V.; Petrauskas, V.; Norvaišas, P.; Lingė, D.; Gibieža, P.; Capkauskaitė, E.; Zakšauskas, A.; Kazlauskas, E.; Manakova, E.; Gražulis, S.; Ladbury, J. E.; Matulis, D. Discovery and Characterization of Novel Selective Inhibitors of Carbonic Anhydrase IX. *J. Med. Chem.* **2014**, *57* (22), 9435−9446.
(10) Linkuvienė, V.; Zubrienė, A.; Manakova, E.; Petrauskas, V.; Baranauskienė, L.; Zakšauskas, A.; Smirnov, A.; Gražulis, S.; Ladbury, J. E.; Matulis, D. Thermodynamic, Kinetic, and Structural Parameterization of Human Carbonic Anhydrase Interactions toward Enhanced Inhibitor Design. *Q. Rev. Biophys.* **2018**, *51*, No. e10.
(11) Matulis, D. *Carbonic Anhydrase as Drug Target: Thermodynamics and Structure of Inhibitor Binding*; Springer Nature, 2019.
(12) Lin, C.-M.; Usama, S. M.; Burgess, K. Site-Specific Labeling of Proteins with Near-IR Heptamethine Cyanine Dyes. *Molecules* **2018**, *23* (11), 2900.
(13) Hu, X.-X.; Su, Y.-T.; Ma, Y.-W.; Zhan, X.-Q.; Zheng, H.; Jiang, Y.-B. A near Infrared Colorimetric and Fluorometric Probe for Organophosphorus Nerve Agent Mimics by Intramolecular Amidation. *Chem. Commun.* **2015**, *51* (82), 15118−15121.
(14) Hu, Z.; Li, R.; Cui, X.; Hu, C.; Chen, Z. A pH-sensitive carbonic anhydrase IX-targeted near-infrared probe for fluorescent sensing and imaging of hypoxic osteosarcoma. *Sens. Actuators, B* **2023**, *379*, 133171.
(15) Zakšauskas, A.; Čapkauskaitė, E.; Jezepčikas, L.; Linkuvienė, V.; Paketurytė, V.; Smirnov, A.; Leitans, J.; Kazaks, A.; Dvinskis, E.; Manakova, E.; Gražulis, S.; Tars, K.; Matulis, D. Halogenated and Di-Substituted Benzenesulfonamides as Selective Inhibitors of Carbonic Anhydrase Isoforms. *Eur. J. Med. Chem.* **2020**, *185*, 111825.
(16) Matulienė, J.; Žvinys, G.; Petrauskas, V.; Kvietkauskaitė, A.; Zakšauskas, A.; Shubin, K.; Zubrienė, A.; Baranauskienė, L.; Kačenauskaitė, L.; Kopanchuk, S.; Veiksina, S.; Paketurytė-Latvė, V.; Smirnovienė, J.; Juozapaitienė, V.; Mickevičiūtė, A.; Michailovienė, V.; Jachno, J.; Stravinskienė, D.; Sližienė, A.; Petrošiūtė, A.; Becker, H. M.; Kazokaitė-Adomaitienė, J.; Yaromina, A.; Čapkauskaitė, E.; Rinken, A.; Dudutienė, V.; Dubois, L. J.; Matulis, D. Picomolar Fluorescent Probes for Compound Affinity Determination to Carbonic Anhydrase IX Expressed in Live Cancer Cells. *Sci. Rep.* **2022**, *12* (1), 17644.
(17) Petrauskas, V.; et al. Thermal Shift Assay for Protein-Ligand Dissociation Constant Determination. *Trends Anal. Chem.* **2024**, *170*, 117417.
(18) Oosterwdk, E.; Ruiter, D. J.; Hoedemaeker, P. J.; Pauwels, E. K.; Jonas, U.; Zwartendijk, I.; Warnaar, S. O. Monoclonal Antibody G 250 Recognizes a Determinant Present in Renal-Cell Carcinoma and Absent from Normal Kidney. *Int. J. Cancer* **1986**, *38* (4), 489−494.
(19) Pastorek, J.; Pastoreková, S.; Callebaut, I.; Mornon, J. P.; Zelník, V.; Opavský, R.; Zat'ovicová, M.; Liao, S.; Portetelle, D.; Stanbridge, E. J. Cloning and Characterization of MN, a Human Tumor-Associated Protein with a Domain Homologous to Carbonic Anhydrase and a Putative Helix-Loop-Helix DNA Binding Segment. *Oncogene* **1994**, *9* (10), 2877−2888.
(20) Saarnio, J.; Parkkila, S.; Parkkila, A.-K.; Haukipuro, K.; Pastoreková, S.; Pastorek, J.; Kairaluoma, M. I.; Karttunen, T. J. Immunohistochemical Study of Colorectal Tumors for Expression of a Novel Transmembrane Carbonic Anhydrase, MN/CA IX, with Potential Value as a Marker of Cell Proliferation. *Am. J. Pathol.* **1998**, *153* (1), 279−285.
(21) Dubois, L.; Douma, K.; Supuran, C. T.; Chiu, R. K.; van Zandvoort, M. A.; Pastorekova, S.; Scozzafava, A.; Wouters, B. G.; Lambin, P. Imaging the Hypoxia Surrogate Marker CA IX Requires Expression and Catalytic Activity for Binding Fluorescent Sulfonamide Inhibitors. *Radiother. Oncol.* **2007**, *83* (3), 367−373.
(22) Ahlskog, J. K.; Schliemann, C.; Marlind, J.; Qureshi, U.; Ammar, A.; Pedley, R. B.; Neri, D. Human Monoclonal Antibodies Targeting Carbonic Anhydrase IX for the Molecular Imaging of Hypoxic Regions in Solid Tumours. *Br. J. Cancer* **2009**, *101* (4), 645−657.
(23) Dubois, L.; Lieuwes, N. G.; Maresca, A.; Thiry, A.; Supuran, C. T.; Scozzafava, A.; Wouters, B. G.; Lambin, P. Imaging of CA IX with Fluorescent Labelled Sulfonamides Distinguishes Hypoxic and (Re)-Oxygenated Cells in a Xenograft Tumour Model. *Radiother. Oncol.* **2009**, *92* (3), 423−428.
(24) Bao, B.; Groves, K.; Zhang, J.; Handy, E.; Kennedy, P.; Cuneo, G.; Supuran, C. T.; Yared, W.; Rajopadhye, M.; Peterson, J. D. In Vivo Imaging and Quantification of Carbonic Anhydrase IX Expression as an Endogenous Biomarker of Tumor Hypoxia. *PLoS One* **2012**, *7* (11), No. e50860.
(25) Tafreshi, N. K.; Bui, M. M.; Bishop, K.; Lloyd, M. C.; Enkemann, S. A.; Lopez, A. S.; Abrahams, D.; Carter, B. W.; Vagner, J.; Grobmyer, S. R.; Gillies, R. J.; Morse, D. L. Noninvasive Detection of Breast Cancer Lymph Node Metastasis Using Carbonic Anhydrases IX and XII Targeted Imaging Probes. *Clin. Cancer Res.* **2012**, *18* (1), 207−219.
(26) Lu, G.; Hillier, S. M.; Maresca, K. P.; Zimmerman, C. N.; Eckelman, W. C.; Joyal, J. L.; Babich, J. W. Synthesis and SAR of Novel Re/99mTc-Labeled Benzenesulfonamide Carbonic Anhydrase IX Inhibitors for Molecular Imaging of Tumor Hypoxia. *J. Med. Chem.* **2013**, *56* (2), 510−520.
(27) Rana, S.; Nissen, F.; Lindner, T.; Altmann, A.; Mier, W.; Debus, J.; Haberkorn, U.; Askoxylakis, V. Screening of a Novel Peptide Targeting the Proteoglycan-like Region of Human Carbonic Anhydrase IX. *Mol. Imaging* **2013**, *12* (8), 7290.2013.00066.
(28) Cheal, S. M.; Punzalan, B.; Doran, M. G.; Evans, M. J.; Osborne, J. R.; Lewis, J. S.; Zanzonico, P.; Larson, S. M. Pairwise Comparison of 89Zr- and 124I-Labeled cG250 Based on Positron Emission Tomography Imaging and Nonlinear Immunokinetic Modeling: In Vivo Carbonic Anhydrase IX Receptor Binding and Internalization in Mouse Xenografts of Clear-Cell Renal Cell Carcinoma. *Eur. J. Nucl. Med. Mol. Imaging* **2014**, *41* (5), 985−994.
(29) Doss, M.; Kolb, H. C.; Walsh, J. C.; Mocharla, V. P.; Zhu, Z.; Haka, M.; Alpaugh, R. K.; Chen, D. Y. T.; Yu, J. Q. Biodistribution and Radiation Dosimetry of the Carbonic Anhydrase IX Imaging Agent [(18) F]VM4−037 Determined from PET/CT Scans in Healthy Volunteers. *Mol. Imaging Biol.* **2014**, *16* (5), 739−746.
(30) Pan, J.; Lau, J.; Mesak, F.; Hundal, N.; Pourghiasian, M.; Liu, Z.; Bénard, F.; Dedhar, S.; Supuran, C. T.; Lin, K.-S. Synthesis and Evaluation of ^{18}F-Labeled Carbonic Anhydrase IX Inhibitors for Imaging with Positron Emission Tomography. *J. Enzyme Inhib. Med. Chem.* **2014**, *29* (2), 249−255.
(31) Sneddon, D.; Poulsen, S.-A. Agents Described in the Molecular Imaging and Contrast Agent Database for Imaging Carbonic Anhydrase IX Expression. *J. Enzyme Inhib. Med. Chem.* **2014**, *29* (5), 753−763.
(32) Dilworth, J. R.; Pascu, S. I.; Waghorn, P. A.; Vullo, D.; Bayly, S. R.; Christlieb, M.; Sun, X.; Supuran, C. T. Synthesis of Sulfonamide Conjugates of Cu(Ii), Ga(Iii), In(Iii), Re(v) and Zn(Ii) Complexes: Carbonic Anhydrase Inhibition Studies and Cellular Imaging Investigations. *Dalton Trans.* **2015**, *44* (11), 4859−4873.
(33) Muselaers, C. H. J.; Rijpkema, M.; Bos, D. L.; Langenhuijsen, J. F.; Oyen, W. J. G.; Mulders, P. F. A.; Oosterwijk, E.; Boerman, O. C.

Radionuclide and Fluorescence Imaging of Clear Cell Renal Cell Carcinoma Using Dual-Labeled Anti-Carbonic Anhydrase IX Antibody G250. *J. Urol.* **2015**, *194*, 532−538.
(34) Peeters, S. G. J. A.; Dubois, L.; Lieuwes, N. G.; Laan, D.; Mooijer, M.; Schuit, R. C.; Vullo, D.; Supuran, C. T.; Eriksson, J.; Windhorst, A. D.; Lambin, P. [(18)F]VM4−037 MicroPET Imaging and Biodistribution of Two In Vivo CAIX-Expressing Tumor Models. *Mol. Imaging Biol.* **2015**, *17*, 615−619.
(35) Srinivasarao, M.; Galliford, C. V.; Low, P. S. Principles in the Design of Ligand-Targeted Cancer Therapeutics and Imaging Agents. *Nat. Rev. Drug Discovery* **2015**, *14* (3), 203−219.
(36) Yang, X.; Minn, I.; Rowe, S. P.; Banerjee, S. R.; Gorin, M. A.; Brummet, M.; Lee, H. S.; Koo, S. M.; Sysa-Shah, P.; Mease, R. C.; Nimmagadda, S.; Allaf, M. E.; Pomper, M. G. Imaging of Carbonic Anhydrase IX with an 111In-Labeled Dual-Motif Inhibitor. *Oncotarget* **2015**, *6* (32), 33733−33742.
(37) Garousi, J.; Honarvar, H.; Andersson, K. G.; Mitran, B.; Orlova, A.; Buijs, J.; Löfblom, J.; Frejd, F. Y.; Tolmachev, V. Comparative Evaluation of Affibody Molecules for Radionuclide Imaging of in Vivo Expression of Carbonic Anhydrase IX. *Mol. Pharmaceutics* **2016**, *13* (11), 3676−3687.
(38) Lv, P.-C.; Putt, K. S.; Low, P. S. Evaluation of Nonpeptidic Ligand Conjugates for SPECT Imaging of Hypoxic and Carbonic Anhydrase IX-Expressing Cancers. *Bioconjugate Chem.* **2016**, *27* (7), 1762−1769.
(39) Tafreshi, N. K.; Lloyd, M. C.; Proemsey, J. B.; Bui, M. M.; Kim, J.; Gillies, R. J.; Morse, D. L. Evaluation of CAIX and CAXII Expression in Breast Cancer at Varied O2 Levels: CAIX Is the Superior Surrogate Imaging Biomarker of Tumor Hypoxia. *Mol. Imaging Biol.* **2016**, *18* (2), 219−231.
(40) Janoniene, A.; Liu, Z.; Baranauskiene, L.; Mäkilä, E.; Ma, M.; Salonen, J.; Hirvonen, J.; Zhang, H.; Petrikaite, V.; Santos, H. A. A Versatile Carbonic Anhydrase IX Targeting Ligand-Functionalized Porous Silicon Nanoplatform for Dual Hypoxia Cancer Therapy and Imaging. *ACS Appl. Mater. Interfaces* **2017**, *9* (16), 13976−13987.
(41) Mahalingam, S. M.; Chu, H.; Liu, X.; Leamon, C. P.; Low, P. S. Carbonic Anhydrase IX-Targeted Near-Infrared Dye for Fluorescence Imaging of Hypoxic Tumors. *Bioconjugate Chem.* **2018**, *29*, 3320−3331.
(42) More, K. N.; Lee, J. Y.; Kim, D.-Y.; Cho, N.-C.; Pyo, A.; Yun, M.; Kim, H. S.; Kim, H.; Ko, K.; Park, J.-H.; Chang, D.-J. Acetazolamide-Based [18F]-PET Tracer: In Vivo Validation of Carbonic Anhydrase IX as a Sole Target for Imaging of CA-IX Expressing Hypoxic Solid Tumors. *Bioorg. Med. Chem. Lett.* **2018**, *28* (5), 915−921.
(43) Espedal, H.; Fonnes, T.; Fasmer, K. E.; Krakstad, C.; Haldorsen, I. S. Imaging of Preclinical Endometrial Cancer Models for Monitoring Tumor Progression and Response to Targeted Therapy. *Cancers* **2019**, *11* (12), 1885.
(44) Huizing, F. J.; Garousi, J.; Lok, J.; Franssen, G.; Hoeben, B. A. W.; Frejd, F. Y.; Boerman, O. C.; Bussink, J.; Tolmachev, V.; Heskamp, S. CAIX-Targeting Radiotracers for Hypoxia Imaging in Head and Neck Cancer Models. *Sci. Rep.* **2019**, *9* (1), 18898.
(45) Kularatne, S. A.; Thomas, M.; Myers, C. H.; Gagare, P.; Kanduluru, A. K.; Crian, C. J.; Cichocki, B. N. Evaluation of Novel Prostate-Specific Membrane Antigen-Targeted Near-Infrared Imaging Agent for Fluorescence-Guided Surgery of Prostate Cancer. *Clin. Cancer Res.* **2019**, *25* (1), 177−187.
(46) van Oostenbrugge, T. J.; Langenhuijsen, J. F.; Oosterwijk, E.; Boerman, O. C.; Jenniskens, S. F.; Oyen, W. J. G.; Fütterer, J. J.; Mulders, P. F. A. Follow-up Imaging after Cryoablation of Clear Cell Renal Cell Carcinoma Is Feasible Using Single Photon Emission Computed Tomography with 111In-Girentuximab. *Eur. J. Nucl. Med. Mol. Imaging* **2020**, *47*, 1864−1870.
(47) Iikuni, S.; Kitano, A.; Watanabe, H.; Shimizu, Y.; Ono, M. Synthesis and Evaluation of Novel Technetium-99m-Hydroxamamide Complex Based on Imidazothiadiazole Sulfonamide Targeting Carbonic Anhydrase-IX for Tumor Imaging. *Bioorg. Med. Chem. Lett.* **2020**, *30* (22), 127596.
(48) Iikuni, S.; Okada, Y.; Shimizu, Y.; Watanabe, H.; Ono, M. Synthesis and Evaluation of Indium-111-Labeled Imidazothiadiazole Sulfonamide Derivative for Single Photon Emission Computed Tomography Imaging Targeting Carbonic Anhydrase-IX. *Bioorg. Med. Chem. Lett.* **2020**, *30* (14), 127255.
(49) Iikuni, S.; Watanabe, H.; Shimizu, Y.; Nakamoto, Y.; Ono, M. PET Imaging and Pharmacological Therapy Targeting Carbonic Anhydrase-IX High-Expressing Tumors Using US2 Platform Based on Bivalent Ureidosulfonamide. *PLoS One* **2020**, *15* (12), No. e0243327.
(50) Patel, S. S.; Rodig, S. J. Overview of Tissue Imaging Methods. In *Biomarkers for Immunotherapy of Cancer: Methods and Protocols* Thurin, M., Cesano, A., Marincola, F. M., Eds.; Methods in Molecular Biology; Springer: New York, NY, 2020; pp 455−465..
(51) Biagiotti, G.; Angeli, A.; Giacomini, A.; Toniolo, G.; Landini, L.; Salerno, G.; Di Cesare Mannelli, L.; Ghelardini, C.; Mello, T.; Mussi, S.; Ravelli, C.; Marelli, M.; Cicchi, S.; Menna, E.; Ronca, R.; Supuran, C. T.; Richichi, B. Glyco-Coated CdSe/ZnS Quantum Dots as Nanoprobes for Carbonic Anhydrase IX Imaging in Cancer Cells. *ACS Appl. Nano Mater.* **2021**, *4* (12), 14153−14160.
(52) van Lith, S. A. M.; Huizing, F. J.; Franssen, G. M.; Hoeben, B. A. W.; Lok, J.; Doulkeridou, S.; Boerman, O. C.; Gotthardt, M.; van Bergen en Henegouwen, P. M. P.; Bussink, J.; Heskamp, S. Novel VHH-Based Tracers with Variable Plasma Half-Lives for Imaging of CAIX-Expressing Hypoxic Tumor Cells. *Mol. Pharm.* **2022**, *19*, 3511−3520.
(53) Du, M.; Liang, T.; Gu, X.; Liu, Y.; Wang, N.; Zhou, W.; Xie, C.; Fan, Q. Carbonic Anhydrase Inhibitor-Decorated Semiconducting Oligomer Nanoparticles for Active-Targeting NIR-II Fluorescence Tumor Imaging. *Nanotechnology* **2023**, *34* (48), 485101.
(54) Hofman, M. S.; Tran, B.; Feldman, D. R.; Pokorska-Bocci, A.; Pichereau, S.; Wessen, J.; Haskali, M. B.; Sparks, R. B.; Vlasyuk, O.; Galetic, I. First-in-Human Safety, Imaging, and Dosimetry of a Carbonic Anhydrase IX-Targeting Peptide, [68Ga]Ga-DPI-4452, in Patients with Clear Cell Renal Cell Carcinoma. *J. Nucl. Med.* **2024**, *65*, 740−743.
(55) Low, P. S.; Marks, I. J.; Gardeen, S.; Kularatne, S. A. FBSA-Based Therapeutic and Radioimaging Conjugates Targeting Carbonic Anhydrase Positive Cancers. U.S. Patent 11,524,082 B2, December 13, 2022. https://patents.google.com/patent/US11524082B2/en (accessed 2024-01-24).
(56) Copeland, R. A. *Evaluation of Enzyme Inhibitors in Drug Discovery: A Guide for Medicinal Chemists and Pharmacologists*; John Wiley & Sons, 2013.
(57) Gedgaudas, M.; Baronas, D.; Kazlauskas, E.; Petrauskas, V.; Matulis, D. Thermott: A Comprehensive Online Tool for Protein-Ligand Binding Constant Determination. *Drug Discovery Today* **2022**, *27* (8), 2076−2079.